

## Enhancing the potency of antimicrobial peptides through molecular engineering and self-assembly

Lucia Lombardi, Yejiao Shi, Annarita Falanga, Emilia Galdiero, Elisabetta de Alteriis, Gianluigi Franci, Igor Chourpa, Helena S. Azevedo, and Stefania Galdiero

*Biomacromolecules*, **Just Accepted Manuscript** • DOI: 10.1021/acs.biomac.8b01740 • Publication Date (Web): 08 Feb 2019

Downloaded from <http://pubs.acs.org> on February 11, 2019

### Just Accepted

“Just Accepted” manuscripts have been peer-reviewed and accepted for publication. They are posted online prior to technical editing, formatting for publication and author proofing. The American Chemical Society provides “Just Accepted” as a service to the research community to expedite the dissemination of scientific material as soon as possible after acceptance. “Just Accepted” manuscripts appear in full in PDF format accompanied by an HTML abstract. “Just Accepted” manuscripts have been fully peer reviewed, but should not be considered the official version of record. They are citable by the Digital Object Identifier (DOI®). “Just Accepted” is an optional service offered to authors. Therefore, the “Just Accepted” Web site may not include all articles that will be published in the journal. After a manuscript is technically edited and formatted, it will be removed from the “Just Accepted” Web site and published as an ASAP article. Note that technical editing may introduce minor changes to the manuscript text and/or graphics which could affect content, and all legal disclaimers and ethical guidelines that apply to the journal pertain. ACS cannot be held responsible for errors or consequences arising from the use of information contained in these “Just Accepted” manuscripts.

1  
2  
3  
4  
5  
6  
7  
8  
9  
10  
11  
12  
13  
14  
15  
16  
17  
18  
19  
20  
21  
22  
23  
24  
25  
26  
27  
28  
29  
30  
31  
32  
33  
34  
35  
36  
37  
38  
39  
40  
41  
42  
43  
44  
45  
46  
47  
48  
49  
50  
51  
52  
53  
54  
55  
56  
57  
58  
59  
60

# Enhancing the potency of antimicrobial peptides through molecular engineering and self-assembly

*Lucia Lombardi,<sup>a,b</sup> Yejiao Shi,<sup>b</sup> Annarita Falanga,<sup>c,d</sup> Emilia Galdiero,<sup>e</sup> Elisabetta de*

*Alteriis,<sup>e</sup> Gianluigi Franci,<sup>f</sup> Igor Chourpa,<sup>g</sup> Helena S. Azevedo,<sup>b</sup> Stefania Galdiero<sup>a,c\*</sup>*

a Department of Pharmacy, School of Medicine, University of Naples Federico II, Via

Mezzocannone 16, 80134, Naples, Italy; stefania.galdiero@unina.it

b School of Engineering and Materials Science, Queen Mary, University of London, Mile

End Road, London E1 4NS, UK

c CIRPEB University of Naples Federico II, Via Mezzocannone 16, 80134, Naples, Italy

d Department of Agricultural Science, University of Naples Federico II, via Università

100, 80055, Portici, Napoli, Italy

1  
2  
3 e Department of Biology, University of Naples Federico II, via Cinthia, 80100, Naples,  
4  
5  
6

7 Italy  
8  
9

10  
11 f Department of Experimental Medicine, University of Campania Luigi Vanvitelli, via  
12  
13

14 Costantinopoli 16, Naples, Italy  
15  
16  
17

18  
19 g Université François-Rabelais de Tours, EA 6295 Nanomédicaments et Nanosondes,  
20  
21

22 31 avenue Monge, 37000 Tours, France  
23  
24  
25  
26

27 **KEYWORDS:** self-assembled, peptide nanostructures, antibacterial nanostructures.  
28  
29  
30  
31  
32  
33  
34  
35  
36

## 37 **ABSTRACT**

38  
39  
40  
41

42 Healthcare-associated infections resulting from bacterial attachment and biofilm  
43  
44 formation on medical implants are posing significant challenges in particular with the  
45  
46 emergence of bacterial resistance to antibiotics. Here, we report the design, synthesis  
47  
48 and characterization of self-assembled nanostructures, which integrate on their surface  
49  
50 antibacterial peptides. The antibacterial WMR peptide, which is a modification of the  
51  
52  
53  
54  
55  
56  
57  
58  
59  
60

1  
2  
3 native sequence of the myxinidin, a marine peptide isolated from the epidermal mucus of  
4  
5  
6  
7 hagfish, was used considering its enhanced activity against Gram-negative bacteria.  
8  
9

10 WMR was linked to a peptide segment of aliphatic residues (AAAAAAA) containing a  
11  
12  
13  
14 lipidic tail ( $C_{19}H_{38}O_2$ ) attached to the  $\epsilon$ -amino of a terminal lysine to generate a peptide  
15  
16  
17 amphiphile (WMR PA). The self-assembly of the WMR PA alone, or combined with co-  
18  
19  
20  
21 assembling shorter PAs, was studied using spectroscopy and microscopy techniques.  
22  
23

24 The designed PAs were shown to self-assemble into stable nanofiber structures and  
25  
26  
27 these nanoassemblies significantly inhibit biofilm formation and eradicate the already  
28  
29  
30  
31 formed biofilms of *P. aeruginosa* (Gram-negative bacteria) and *C. albicans* (pathogenic  
32  
33  
34 fungus) when compared to the native WMR peptide. Our results provide insights into the  
35  
36  
37  
38 design of peptide based supramolecular assemblies with antibacterial activity, and  
39  
40  
41  
42 establish an innovative strategy to develop self-assembled antimicrobial materials for  
43  
44  
45 biomedical applications.  
46  
47  
48  
49  
50  
51  
52  
53  
54  
55  
56  
57  
58  
59  
60

## 1 INTRODUCTION

The extensive use and misuse of antibiotics for human and animal care have resulted in the development of antibiotic resistant bacteria, which is a major global health problem.<sup>1</sup>

The emergence of resistant bacteria calls for the development of new classes of antimicrobial agents to avoid getting back to the pre-antibiotic era. Severe infections are also frequently associated to biomedical implants (prosthetics, catheters etc.) which have revolutionized medicine but provide an optimal surface for biofilm formation.<sup>2</sup>

Furthermore, once developed, biofilms are difficult to treat with standard therapeutic regimens and pose a significant clinical problem with medical devices. Biofilm may be composed of single or multiple species of bacteria and fungi, forming a complex three-dimensional architecture embedded in a self-produced exopolymeric matrix, which renders more difficulties for the antibiotic to penetrate into the matrix and eradicate the pathogenic microorganisms.<sup>3</sup> Managing and preventing biofilm formation is challenging, but can be addressed using materials combined with micro/nanotechnologies.

1  
2  
3  
4 Recently, great attention has been devoted to peptides with the ability to self-assemble  
5  
6  
7 into pre-defined structures and opportunity to integrate multiple biological functionalities  
8  
9  
10 for diverse applications from materials to biomedical sciences.<sup>4-5</sup> Thanks to the proven  
11  
12  
13 biocompatibility of peptides, their design flexibility and easy modification by functional  
14  
15  
16 groups, self-assembly of peptides offers the possibility to generate highly stable  
17  
18  
19 nanostructures combining different functional elements through individually weak non-  
20  
21  
22 covalent interactions.<sup>4-5</sup>  
23  
24  
25  
26  
27

28 In the context of biomedical applications, the development of self-assembling peptides  
29  
30  
31 with antibacterial activity has not been widely exploited, although self-assembly is used  
32  
33  
34 by nature to fight infections.<sup>6</sup> Most antimicrobial peptides<sup>7</sup> (AMPs) are natural agents  
35  
36  
37 produced by both plants and animals, and can self-assemble into fibrillar amyloid-like  
38  
39  
40 nanostructures. They interact with the membranes of bacteria and exert their antimicrobial  
41  
42  
43 activity by causing membrane damage, being natural weapons for combating microbial  
44  
45  
46 infections.<sup>1, 8-11</sup> Recently, several studies have been carried out on self-assembling  
47  
48  
49 materials to provide model systems for the development of antibacterial agents. In spite  
50  
51  
52 of these interests in self-assembling peptides with antibacterial activity, most studies are  
53  
54  
55  
56  
57  
58  
59  
60

1  
2  
3 limited to self-assembling entities to verify their eventual antibacterial activity.<sup>12-14</sup> For  
4  
5  
6  
7 example, the antibacterial activity of self-assembled diphenylalanine was recently  
8  
9  
10 reported, showing that the diphenylalanine nano-assemblies can inhibit bacterial growth  
11  
12  
13 and damage bacterial morphology at a concentration of approximately 400  $\mu\text{mol/mL}$ .<sup>15</sup>  
14  
15  
16  
17 The development of this minimal model of antibacterial materials provides a starting point  
18  
19  
20  
21 for engineering more potent self-assembled nanosystems.  
22  
23

24 In this context, integrating antimicrobial peptides<sup>9</sup> into a self-assembling system offers  
25  
26  
27 the opportunity to engineer their antimicrobial activity against a wide range of Gram-  
28  
29  
30 positive and Gram-negative bacteria, while reducing haemolysis and allergic responses  
31  
32  
33 and potentially the development of resistance.<sup>16</sup> Moreover, particularly attracting is the  
34  
35  
36 possibility to combine multiple components, including AMPs and conventional antibiotics,  
37  
38  
39 which may assist in reducing both the administration dose of the antibiotic and the  
40  
41  
42 development of resistance. The antibacterial properties of AMPs and the possibility to  
43  
44  
45 display them on the surface of self-assembled nanostructures may provide a more  
46  
47  
48 effective way to enhance the activity of AMPs, establishing an innovative design principle  
49  
50  
51  
52 for the development of antibacterial materials. Furthermore, improved biocompatibility is  
53  
54  
55  
56  
57  
58  
59  
60

1  
2  
3 also expected by reducing toxic effects for human cells.<sup>17-19</sup> The multivalent presentation  
4  
5  
6  
7 of AMPs on the surface of supramolecular nanostructures provides significant  
8  
9  
10 improvements compared to the activity of single soluble peptides. It aids in increasing the  
11  
12  
13 stability and half-life of peptides, while augmenting and controlling the local concentration  
14  
15  
16  
17 of the active peptides, which enables their enhanced interactions with bacteria.  
18  
19

20  
21 The spontaneous organization of molecules into ordered aggregates through  
22  
23  
24 supramolecular interactions, known as self-assembly, can be achieved by the rational  
25  
26  
27 design of individual molecules. Peptide amphiphiles (PAs), molecules containing a hydrocarbon  
28  
29  
30 chain attached to a peptide segment, are known to self-assemble into cylindrical nanostructures.<sup>20</sup>  
31  
32  
33 PAs offer a versatile self-assembling platform to build supramolecular nanomaterials with  
34  
35  
36 demonstrated biomedical applications. Different PA molecules have been designed and exploited  
37  
38 by numerous research groups, including the labs from Stupp, Tirrell, Deming, Guler, Hamley, and  
39  
40 others.<sup>20-29</sup>  
41

42  
43 As proof of concept, we selected the antimicrobial peptide WMR, which has been  
44  
45  
46 previously identified in our lab as a modification of the native sequence of myxinidin, as  
47  
48  
49 the key functionality to be displayed in the self-assembled nanomaterials.<sup>30-32</sup> Myxinidin  
50  
51  
52  
53 is a marine antimicrobial peptide isolated from the epidermal mucus of hagfish (*Myxine*  
54  
55  
56  
57  
58  
59  
60



1  
2  
3  
4 *glutinosa* L.).<sup>33-34</sup> It is one of the shortest AMPs discovered so far (12-amino-acid peptide:  
5  
6  
7 NH<sub>2</sub>-GIHDILKYGKPS-CONH<sub>2</sub>) with potent antibacterial activity against a wide range of  
8  
9  
10 bacteria and yeast pathogens.<sup>33-34</sup> The peptide WMR (13-amino-acid-peptide: NH<sub>2</sub>-  
11  
12  
13 WGIRRILKYGKRS-CONH<sub>2</sub>) contains one more tryptophan residue at the N-terminus and  
14  
15  
16 a higher number of positively charged amino acids (arginine), compared to the native  
17  
18  
19 sequence. These features are essential for its greater antimicrobial activity against  
20  
21  
22  
23  
24 *Pseudomonas aeruginosa* as found in previously reported activity and structural  
25  
26  
27 studies.<sup>30-32</sup>

31  
32 This work focuses on the possibility of exploiting the multivalent presentation of AMPs  
33  
34  
35 on self-assembled nanostructures to improve anti-biofilm activities of two representative  
36  
37  
38 species of unresolved medical impact: the Gram-negative bacterium *P. aeruginosa* and  
39  
40  
41 the fungus *Candida albicans*.<sup>35-36</sup> The pathogenicity of these species is related to their  
42  
43  
44 capability to form structured biofilms on both biotic (mucosae) and abiotic (medical  
45  
46  
47 devices) surfaces. In particular, *P. aeruginosa* biofilms are responsible for most lung  
48  
49  
50 infections<sup>37</sup> and colonization of medical devices is the leading cause of acute nosocomial  
51  
52  
53 pneumonia or sepsis.<sup>38</sup> Furthermore, *C. albicans*, which is the prevalent fungal species  
54  
55  
56  
57  
58  
59  
60

1  
2  
3 of the healthy human microbiota, also forms biofilms, causing localized or even  
4  
5  
6  
7 disseminated infections especially in immunocompromised patients.<sup>39</sup> Both  
8  
9  
10 *Pseudomonas* and *Candida* biofilms are worldwide diffused and have developed a  
11  
12  
13  
14 widespread resistance to classical antibiotics, and were thus chosen in this study as  
15  
16  
17  
18 model organisms.

19  
20  
21 We propose self-assembling antimicrobial peptides based on the WMR sequence to  
22  
23  
24 enhance their antibacterial efficacy via multivalent display of the AMP sequence. The  
25  
26  
27  
28 antibiofilm activity of self-assembled WMR-based PAs was studied and compared to that  
29  
30  
31 of unmodified WMR. Our nanosystem represents a sound strategy to design smart  
32  
33  
34  
35 materials, which may also contain a conventional antibiotic and be stimuli responsive (e.g.  
36  
37  
38 pH-sensitive), releasing the loaded antibiotic following a change in pH. These  
39  
40  
41  
42 nanostructures hold great promise due to their biocompatibility and biodegradability.

## 43 44 45 46 47 48 49 **2 MATERIALS AND METHODS**

### 50 51 52 *2.1 Peptide synthesis and purification*

53  
54  
55  
56  
57  
58  
59  
60

1  
2  
3  
4 *Materials.* Fmoc-protected amino acid derivatives, coupling reagents, and rink amide p-  
5  
6  
7 methylbenzhydrylamine (MBHA) resin were purchased from Iris Biotech GmbH  
8  
9  
10 (Germany). Other chemicals were purchased from Sigma-Aldrich and DelChimica (Italy).  
11  
12

13  
14 *Peptide synthesis.* The PAs listed in Table 1 were synthesized on a rink amide resin.  
15  
16  
17 The removal of the Fmoc protecting group on the resin and amino acids was performed  
18  
19  
20 with 30% v/v piperidine in DMF for 10 min and the couplings were carried out in the  
21  
22  
23 presence of 4 eq Fmoc-protected amino acid, 4 eq DIC and 4 eq oxymapure (first  
24  
25  
26 coupling) or 4 eq amino acid, 4 eq HATU and 8 eq DIPEA (second coupling).<sup>40-41</sup> A  
27  
28  
29 hydrophobic tail, nonadecanoic acid (C19), was attached to the first lysine at C-terminal  
30  
31  
32 end. This lysine was protected with an Mtt group in the side chain, which was removed  
33  
34  
35 with about 20 washes with DCM:TFA:TIS 94:1:5 of 2 mins each. The free side chain was  
36  
37  
38 then used to attach the tail with 2 eq C19, 2 eq DIC/oxymapure and 4 eq DIPEA in  
39  
40  
41 DMF/THF 80/20 % vol/vol (two overnight couplings). At the end of the synthesis, the  
42  
43  
44 peptide was cleaved from the resin with TFA/thioanisole/anisole/water/EDT  
45  
46  
47 82.5/5/5/5/2.5 % vol, precipitated in ice-cold diethyl ether and purified in a Phenomenex  
48  
49  
50 Jupiter 4 $\mu$ m Proteo 90 Å 250 x 21.20 mm column with a linear gradient of solvent B (0.1%  
51  
52  
53  
54  
55  
56  
57  
58  
59  
60

1  
2  
3 TFA in acetonitrile) in solvent A (0.1% TFA in water) from 20 to 80% in 25 min with UV  
4  
5  
6  
7 detection at 210 nm.  
8  
9

## 10 **2.2 Preparation of peptide self-assemblies**

11  
12  
13  
14 For all the experiments, peptide assemblies were prepared as follows; peptide stock  
15  
16  
17 solutions were prepared by dissolving the single peptides in water, then sonicating for 15  
18  
19  
20 min. Different aliquots were taken to prepare aqueous solutions of the single peptides  
21  
22  
23 (PA1, PA2) or peptide mixtures (PA1+WMR2PA, PA2+WMR2PA) at different  
24  
25  
26 concentrations. In the mixtures, the peptide molar ratio was 1:1 and was kept constant  
27  
28  
29 for all experiments. Then, the solutions were diluted until the concentration was lower  
30  
31  
32 than the critical aggregation concentration and then sonicated for 15 min to break any  
33  
34  
35 type of pre-existing aggregates. All the samples were freeze-dried and hydrated with the  
36  
37  
38 proper volume of water, buffer or dye, in order to obtain the desired concentrations. All  
39  
40  
41 the solutions were left to equilibrate for 1 h.  
42  
43  
44  
45  
46  
47

## 48 **2.3 Critical aggregation concentration (CAC) determination**

49  
50  
51  
52 The solvatochromic fluorescent probe Nile red is widely used to determine the CAC of  
53  
54  
55 self-assembling peptides.<sup>42</sup> Nile red shows a blue shift with decreasing solvent polarity. Since  
56  
57  
58  
59  
60

1  
2  
3 Nile red is poorly soluble in water, there is a large preference to partition aggregates which  
4  
5  
6 offer hydrophobic binding sites. Initially, 1 mM methanolic Nile red was prepared. Then  
7  
8  
9 the methanolic Nile red was diluted with water in order to have a final concentration of  
10  
11  
12 500 nM (solution A). A stock peptide solution (0.5 mM) was prepared by dissolving the  
13  
14  
15 peptide in water (solution B) and different peptide concentrations were prepared using  
16  
17  
18 solution B as a stock and water as diluting solvent. Final solutions were mixed, diluted,  
19  
20  
21 sonicated and freeze-dried. The peptide powders were dissolved with the right volume of  
22  
23  
24 solution A and allowed to stand in the dark place for 1 h before measurement. Emission  
25  
26  
27 spectra for each solution were measured by a Cary Eclipse Varian spectrometer. Spectra  
28  
29  
30 were taken between 570 and 700 nm at a slit width of 5 nm, using an excitation  
31  
32  
33 wavelength of 550 nm and a 10 nm slit width. The measurements were performed in  
34  
35  
36 triplicate. The same experiments were carried out with the mixtures of peptides. The data  
37  
38  
39 were analysed by plotting the maximum emission fluorescence corresponding  
40  
41  
42 wavelength (y) as a function of peptide concentration (x) and fitting with the sigmoidal  
43  
44  
45 Boltzmann equation:<sup>43</sup>  
46  
47  
48  
49  
50  
51  
52  
53  
54  
55  
56  
57  
58  
59  
60

$$y = \frac{A_1 - A_2}{1 + e^{\left(\frac{x - x_0}{\Delta x}\right)}} + A_2$$

where the variable  $A_1$  and  $A_2$  correspond to the upper and lower limits of the sigmoid,  $x_0$  is the inflection point of the sigmoid and  $\Delta x$  is the parameter, which characterizes the steepness of the function. The sigmoidal plot allows calculating the CAC value at  $x_0$ .

## 2.4 Secondary structure analysis

*Circular dichroism (CD) analysis.* CD spectra of PA solutions were recorded from 195 nm to 260 in a Jasco J-810 spectropolarimeter using a 1.0 or 0.1 cm quartz cell at room temperature under a constant flow of nitrogen gas. The 1.0 cm cell was used for samples at concentrations of 2.5  $\mu\text{M}$ , 5  $\mu\text{M}$  and 10  $\mu\text{M}$ , while for the other concentrations the 0.1 cm cell was more suitable for avoiding the excessive increase of HT voltage. Other experimental settings were: scan speed of 5 nm/min, sensitivity of 50 mdeg, time constant of 16 s, bandwidth of 1 nm. Each spectrum was obtained through averaging three scans, and converting the signal to mean molar ellipticity. CD measurements were carried out for the different peptides alone or in combinations at different concentrations, ionic strengths and pHs.

1  
2  
3  
4 *Raman spectroscopy analysis.* Aqueous solutions of the peptides PA1, WMR2PA and  
5  
6  
7 PA2 alone, or in mixtures PA1+WMR2PA and PA2+WMR2PA, were lyophilized and analysed  
8  
9  
10 under a 10 × objective of a LabRam microspectrometer (Horiba SAS, Villeneuve d'Ascq,  
11  
12  
13 France). The latter was equipped with a 690 nm laser excitation source (laser power was  
14  
15  
16 ca 27 mW at the sample), an 1800 gr/mm diffraction grating and an air-cooled CCD  
17  
18  
19 detector. No sample photodegradation was observed during the measurements. Each  
20  
21  
22 spectrum shown is an average of 16 scans of 1 sec. The spectral data acquirement and  
23  
24  
25 treatment were done using a LabSpec software (Horiba SAS, Villeneuve d'Ascq, France)  
26  
27  
28  
29  
30

## 31 **2.5 Morphology Characterization**

32  
33  
34

35 Transmission electron microscopy (TEM) imaging was performed to analyse the  
36  
37  
38 morphology of the self-assembled peptide nanostructures. TEM was performed on JEOL  
39  
40  
41 1230 with an accelerating voltage of 80 kV and images were recorded by using a SIS  
42  
43  
44 Megaview III wide angle CCD camera. Solutions of peptides and their mixtures were  
45  
46  
47  
48 freshly prepared in ultrapure water at a concentration which was higher than their  
49  
50  
51  
52 respective CAC. After ageing for 24 h, the peptide solutions were loaded onto carbon film  
53  
54  
55  
56  
57  
58  
59  
60

1  
2  
3 coated copper grids with 400 mesh and negatively stained by uranyl acetate. The grids  
4  
5  
6  
7 were allowed to dry at room temperature for at least 3 h before collecting the images.  
8  
9

## 10 **2.6 Zeta-potential measurement**

11  
12  
13  
14 The zeta-potential of PA solutions at different concentrations was measured using  
15  
16  
17 Zetasizer Nano-ZS (Malvern Instruments, Worcestershire, UK). All measurements were  
18  
19  
20 performed at 25 °C, at pH 3, 7 and 10 in triplicate, and 1 h after the sample preparations.  
21  
22  
23

## 24 **2.7 Proteolytic stability**

25  
26  
27  
28 Trypsin was added into solutions of WMR and the PA1+WMR2PA or PA2+WMR2PA  
29  
30  
31 mixtures at trypsin/peptide molar ratio of 1/500. The concentration of WMR was 100 µM,  
32  
33  
34 while the mixture was made of two peptides at a molar ratio of 1/1 and at a total peptide  
35  
36  
37 concentration of 200 µM. All the solutions were prepared in 5 mM Tris-base (pH 8) and  
38  
39  
40 incubated at 37 °C. At 1 h, 3 h, 4 h, 24 h and 48 h, 100 µL of the sample solutions were  
41  
42  
43  
44  
45 taken and injected into the analytical reverse phase high performance liquid  
46  
47  
48 chromatography (RP-HPLC, Agilent 1200). The absorbance changes of WMR or  
49  
50  
51 WMR2PA were monitored in comparison to the signals of WMR or WMR2PA, which were  
52  
53  
54  
55 not treated with trypsin. All the solutions were eluted at 1 mL min<sup>-1</sup> using a linear gradient  
56  
57  
58  
59  
60



1  
2  
3 of solvent B (0.1% TFA in acetonitrile) in solvent A (0.1% TFA in water) with UV detection  
4  
5  
6  
7 at 210 nm. In details, WMR was eluted using an isocratic hold at 5% B for 3 min then a  
8  
9  
10 step to 70% B in 15 min, while the complexes PA1+WMR2PA and PA2+WMR2PA were  
11  
12  
13  
14 run with a linear gradient from 20% to 90% B in A in 20 min.  
15  
16

## 17 **2.8 Anti-biofilm activity**

18  
19  
20 Vero cells, *C. albicans* and *P. aeruginosa* were purchased from ATCC, Rockville, (USA). Cell  
21  
22  
23 media were obtained from Gibco, Invitrogen Co. (USA) and Euroclone (Italy). *C. albicans* ATCC  
24  
25  
26 90028 culture grown for 24 h in Triptone Soya Broth medium (TSB) with 1% glucose  
27  
28  
29 (Difco) at 37 °C was centrifuged at 5000 × g (4 °C) for 15 min, washed twice in phosphate  
30  
31  
32 buffered saline (PBS, pH 7.0) and resuspended in RPMI-1640 medium at a density of 1  
33  
34  
35 × 10<sup>6</sup> cells/mL. *P. aeruginosa* ATCC 9027 was grown overnight at 37 °C in TBS, washed  
36  
37  
38 twice in PBS and re-suspended to obtain a suspension equivalent to 1 × 10<sup>5</sup> cells/mL.  
39  
40  
41  
42 100 µL of each culture was dispensed into wells of 96-well polystyrene microtiter plates.  
43  
44  
45

46  
47 To form biofilms at early stage (24 h biofilms), the plates were incubated at 37 °C for 24  
48  
49  
50 h, whereas to generate biofilms at maturation stage (48 h biofilms), the plates were  
51  
52  
53  
54 incubated for 48 h and the medium was renewed after the first 24 h. Amphotericin B and  
55  
56  
57  
58  
59  
60

1  
2  
3 ampicillin were used as positive controls at concentrations ranging from 0.4 to 1.6 mg/mL,  
4  
5  
6  
7 and untreated biofilms served as the growth control. Various concentrations of the test  
8  
9  
10 molecules were prepared in PBS and added to the wells to prevent cells adherence or to  
11  
12  
13  
14 eradicate preformed biofilm.  
15

16  
17 For biofilm mass quantification, the wells were washed twice with PBS, air-dried for 45  
18  
19  
20 min, and stained with 0.4% crystal violet aqueous solution. Absorbance values were read  
21  
22  
23  
24 at 570 nm using a micro-plate reader (SINERGYTM H4, Biotek Instruments, Winooski,  
25  
26  
27 VT, USA BioTek Instruments, Inc). The effect of test molecules on biofilm eradication was  
28  
29  
30  
31 quantified by using the XTT assay that analyses the density of the viable adhered cells  
32  
33  
34  
35 measuring the relative metabolic activity using the XTT [2,3-bis (2-methoxy-4-nitro-5-  
36  
37  
38 sulfophenyl)-5- (phenylamino) carbonyl) -2H-tetrazolium hydroxide] colorimetric assay Kit  
39  
40  
41 (Sigma) following manufacturer's instructions.<sup>44-45</sup>  
42  
43  
44

## 45 **2.9 Biocompatibility for mammalian cells**

46  
47  
48 *Eukaryotic cell cytotoxicity.* Vero cells were exposed to increasing concentrations of  
49  
50  
51  
52 peptides, and the number of viable cells was determined using the 3-(4,5-dimethylthiazol-  
53  
54  
55  
56 2-yl)-2,5-diphenyltetrazolium bromide (MTT) assay that is based on the reduction of the  
57  
58  
59  
60

1  
2  
3  
4 yellowish MTT to the insoluble and dark blue formazan by viable and metabolically active  
5  
6  
7 cells.<sup>46</sup> Vero cells were sub-cultured in 96-well plates at a seeding density of  $2 \times 10^4$   
8  
9  
10 cells/well and treated with peptides at increasing concentrations 1, 20, 50, 100 and 200  
11  
12  
13  $\mu\text{M}$  for 1 and 24 h. The medium was then gently aspirated, MTT solution (5 mg/ml) was  
14  
15  
16 added to each well, and the cells were incubated for further 3 h at 37 °C. The medium  
17  
18  
19 with MTT solution was removed, and the formazan crystals were dissolved with dimethyl  
20  
21  
22 sulfoxide. The absorption values at 570 nm were measured using a TECAN infinite 200  
23  
24  
25 microplate reader (lifesciences.tecan.com). The viability of Vero cells in each well was  
26  
27  
28 presented as a percentage of control cells. All experiments were performed in triplicate  
29  
30  
31 and the average with standard deviation was reported. Cell culture without and with 30%  
32  
33  
34 DMSO were used as the positive and negative controls, respectively.  
35  
36  
37  
38  
39  
40  
41

42 *Haemolytic assay.* The haemolytic activity of the peptides was determined using fresh  
43  
44  
45 human erythrocytes from healthy donors. 25 ml of blood was drawn directly into K2-  
46  
47  
48 EDTA-coated Vacutainer tubes to prevent coagulation. The blood was then centrifuged  
49  
50  
51 at  $500 \times g$  for 5 min, and levels of haematocrits were marked. The plasma was gently  
52  
53  
54 aspirated and replaced with 150 mM NaCl solution. The solution was then inverted and  
55  
56  
57  
58  
59  
60

1  
2  
3 mixed. The samples were centrifuged at  $500 \times g$  for 5 min and resuspended with PBS at  
4  
5  
6  
7 pH 7.4. Then the cells were diluted 1:50 in PBS solution. Peptides were added to the  
8  
9  
10 erythrocyte suspension (5% vol/vol), at a final concentration used in the MTT assay with  
11  
12  
13  
14 a final volume of 100  $\mu$ l. The samples were incubated with agitation at 37 °C for 60 min.  
15  
16  
17 The release of haemoglobin was monitored by measuring the absorbance (Abs) of the  
18  
19  
20 supernatant at 540 nm. The control for zero haemolysis (blank) consisted of erythrocytes  
21  
22  
23  
24 suspended in PBS. Detergent (20% Triton X-10) lysed erythrocytes was used as a  
25  
26  
27 standard for 100% haemolysis. The percentage of haemolysis was calculated using the  
28  
29  
30  
31 following equation:  
32  
33

$$\% \text{ haemolysis} = \frac{Abs_{\text{sample}} - Abs_{\text{blank}}}{Abs_{\text{total lysis}} - Abs_{\text{blank}}} \cdot 100$$

34  
35  
36  
37  
38  
39 All experiments were performed in triplicate and the average with standard deviation  
40  
41  
42 was reported.  
43  
44

## 45 46 **3 RESULTS AND DISCUSSION**

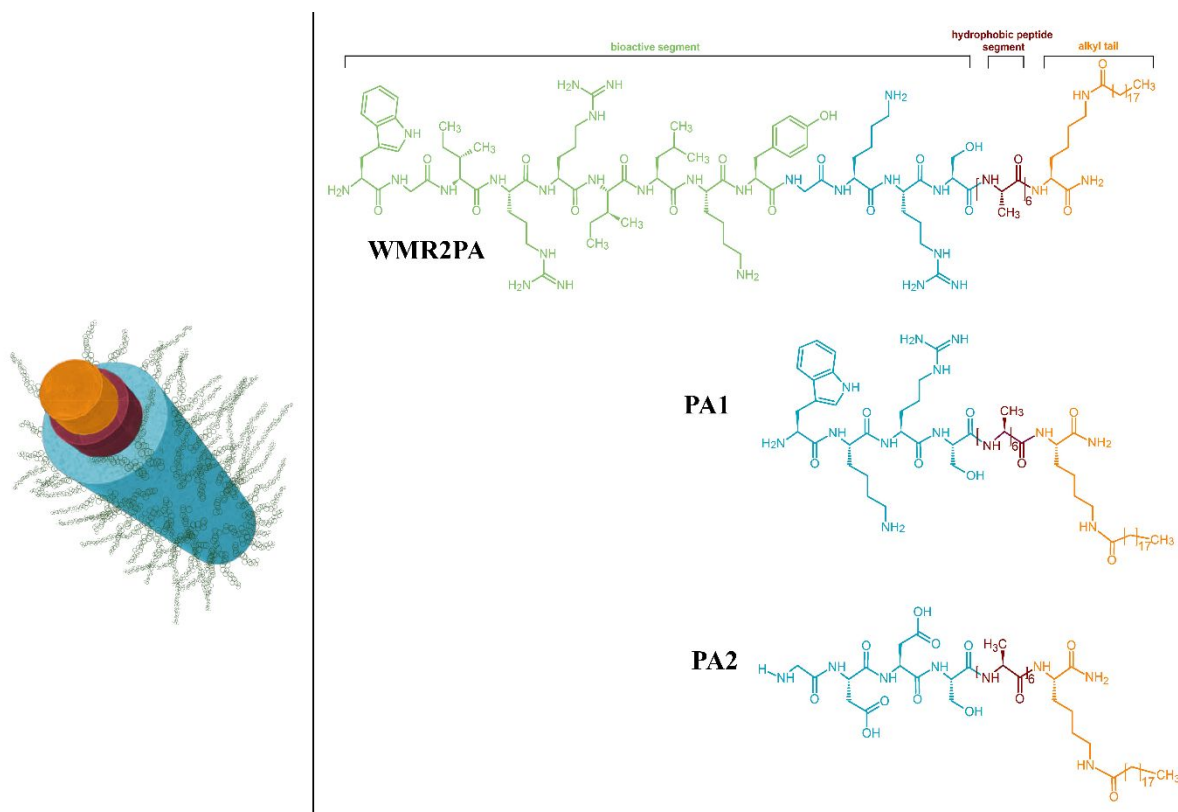
### 47 48 49 **3.1 Peptide design**

50  
51  
52  
53  
54  
55  
56  
57  
58  
59  
60

1  
2  
3 The molecular design employed in this study is based on a PA design (**Figure 1**,  
4 WMR2PA) and consists of a self-assembling segment composed of aliphatic amino acids  
5  
6 (e.g. alanine residues, **Figure 1**, brown segment) and/or lipid tail (**Figure 1**, orange  
7 segment) attached to an AMP sequence (**Figure 1**, green segment). The designed  
8  
9 WMR2PA is expected to self-assemble into cylindrical nanostructures. In such a system,  
10  
11 it would be easy to tune the antibacterial activity by simply changing the AMP sequence  
12  
13 on the surface without modifying the self-assembled nanostructures. In addition, to tune  
14  
15 the density of the AMP sequence displayed on the surface, we used two different shorter  
16  
17 PAs, designed to co-assemble with AMP PA (**Figure 1**, PA1 and PA2). Because  
18  
19 antibacterial activity is attained at low concentrations (Minimal Inhibitory Concentrations  
20  
21 - MICs - around 10  $\mu$ M are considered acceptable for the obtainment of active molecules),  
22  
23 it would not be necessary to develop a structure entirely composed of the AMP sequence.  
24  
25 In this molecular design, different percentages of the antibacterial sequence can be  
26  
27 integrated while the self-assembly is driven by the shorter PAs.  
28  
29  
30  
31  
32  
33  
34  
35  
36  
37  
38  
39  
40  
41  
42  
43  
44  
45  
46  
47  
48  
49  
50

51  
52 The peptide WMR (NH<sub>2</sub>-WGIRRILKYGKRS-CONH<sub>2</sub>) used in this study is a modification  
53  
54 of the native sequence of the myxinidin and shows enhanced activity against *E. coli* (MIC  
55  
56  
57  
58  
59  
60

1  
2  
3  
4  $2 \mu\text{M}$ ) and *P. aeruginosa* (MIC  $2 \mu\text{M}$ ) bacteria.<sup>30-31</sup> Here, several modifications of WMR  
5  
6  
7 were designed.



8  
9  
10  
11  
12  
13  
14  
15  
16  
17  
18  
19  
20  
21  
22  
23  
24  
25  
26  
27  
28  
29  
30  
31  
32  
33  
34  
35  
36  
37  
38  
39  
40  
41 **Figure 1.** Molecular structure of peptide WMR2PA, PA1 and PA2 and their suggested  
42 self-assembled nanostructure.

43  
44  
45  
46  
47  
48  
49  
50  
51  
52 In the first sequence, we added a six alanine sequence at the C-terminus (WMR1PA:  
53  $\text{NH}_2\text{-WGIRRILKYGKRSAAAAAA-CONH}_2$ ) (**Figure 1**, green-turquoise-brown); the  
54  
55  
56  
57  
58  
59  
60

1  
2  
3 aliphatic residues provide a hydrophobic moiety to drive self-assembly.<sup>47-48</sup> However, this  
4  
5  
6  
7 sequence was unable to aggregate at various concentrations and pHs, suggesting that  
8  
9  
10 alanines are not sufficient to promote the aggregation. To increase the hydrophobic  
11  
12  
13 driving force and favour the aggregation of the peptide, NH<sub>2</sub>-WGIRRLKYGKRSAAAAA-  
14  
15  
16  
17 K(C19)-CONH<sub>2</sub> (WMR2PA) was synthesized, which contains a hydrophobic tail on the  
18  
19  
20  
21 side chain of the C-terminal lysine residue (C19, composed of 19 carbon atoms) (**Figure**  
22  
23  
24 **1**, green-turquoise-brown-orange). This peptide was co-assembled with a shorter  
25  
26  
27  
28 sequence bearing a high tendency to aggregate in order to obtain a self-assembled  
29  
30  
31  
32 nanostructure displaying WMR on the surface. We initially designed the short sequence  
33  
34  
35 containing the same sequence as the C-terminal part of WMR2PA and bearing a  
36  
37  
38 tryptophan at the N-terminus to allow detection by fluorescence spectroscopy (PA1: NH<sub>2</sub>-  
39  
40  
41  
42 WKRSAAAAAAK(C19)-CONH<sub>2</sub>). PA1 was characterized alone and in combination with  
43  
44  
45  
46 WMR2PA. To enhance the co-aggregation, a negative version of PA1 was designed  
47  
48  
49 (NH<sub>2</sub>-GDDSAAAAAAK(C19)-CONH<sub>2</sub>) containing aspartic residues and lacking the  
50  
51  
52  
53 tryptophan residue (PA2) which being bulky could hamper the aggregation process. The  
54  
55  
56  
57 negatively charged aspartic acid residues are expected to interact electrostatically with  
58  
59  
60

the positive residues on WMR2PA (lysine, arginine) and promote cohesion among the peptide molecules. The designed peptide sequences are listed in **Table 1** and their chemical structures detailed in **Figure 1**.

<b>Table 1. Sequence and molecular weight (Mw) of the designed peptides</b>		
<b>Name</b>	<b>Sequence</b>	<b>MW (g/mol)</b>
<b>WMR</b>	NH <sub>2</sub> -WGIRRILKYGKRS-CONH <sub>2</sub>	1632.88
<b>WMR1PA</b>	NH <sub>2</sub> -WGIRRILKYGKRSAAAAAA-CONH <sub>2</sub>	2059.45
<b>WMR2PA</b>	NH <sub>2</sub> -WGIRRILKYGKRSAAAAAAK(C19)-CONH <sub>2</sub>	2466.79
<b>PA1</b>	NH <sub>2</sub> -WKRSAAAAAAK(C19)-CONH <sub>2</sub>	1410.14
<b>PA2</b>	NH <sub>2</sub> -GDDSAAAAAAK(C19)-CONH <sub>2</sub>	1226.94

### 3.2 Peptide co-assembly

#### 3.2.1 Critical aggregation concentration (CAC)

Self-assembling capabilities of single PAs and PA mixtures were analysed by a fluorescence assay with the fluorophore Nile red. This fluorophore is poorly water soluble while displaying a large preference to partition in aggregates that offer hydrophobic binding sites and producing a blue shift and hyperchromic effect.



1  
2  
3 The changes of the emission signal of the Nile red is an indication of the aggregate  
4  
5  
6  
7 formation and the concentration at which the changes occur allows the determination of  
8  
9  
10 the CAC.

11  
12  
13  
14 In **Figure 2**, the wavelength of Nile red maximum fluorescence emission at different  
15  
16  
17 concentrations of single peptides is displayed. We used pH 7 (physiological condition) for  
18  
19  
20 all peptides and mixtures.

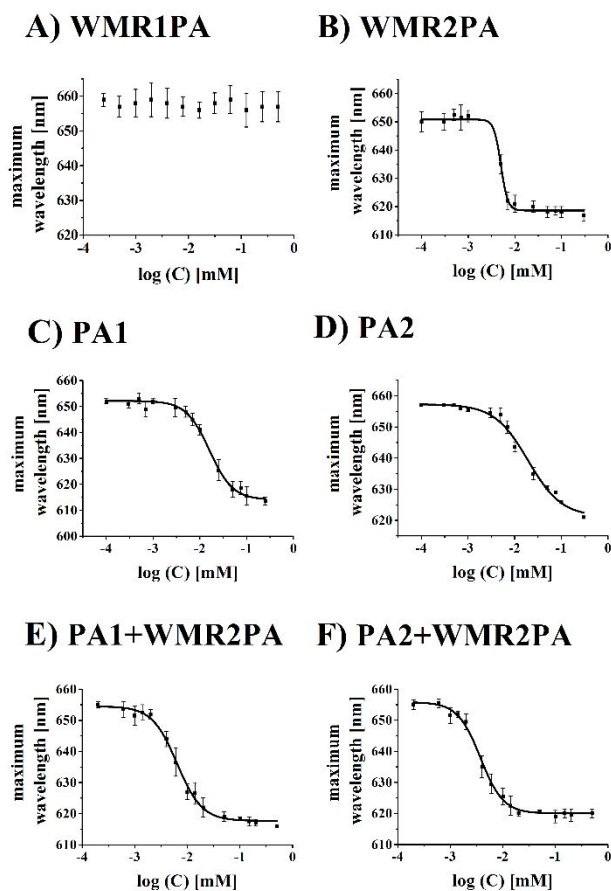
21  
22  
23  
24 For peptide WMR1PA (**Figure 2A**), we were unable to observe any blue shift, indicating  
25  
26  
27 the inability of this peptide to aggregate under the range of concentrations investigated.  
28  
29  
30  
31 The presence of alanines alone was not sufficient to confer the hydrophobic driving force  
32  
33  
34 to promote peptide aggregation.  
35  
36  
37

38  
39 The modified sequence WMR2PA, containing the hydrophobic tail conjugated on the  
40  
41  
42 side chain of the C-terminal lysine, was able to aggregate and a CAC value of 5  $\mu\text{M}$  was  
43  
44  
45 determined (**Figure 2B**).

46  
47  
48  
49 Then, we analysed the aggregation capabilities of the peptides PA1 and PA2, which  
50  
51  
52 were designed to co-assemble with WMR2PA. As shown in **Figure 2C**, peptide PA1 bears  
53  
54  
55  
56  
57  
58  
59  
60

1  
2  
3 a tendency to aggregate and a CAC value of 16  $\mu\text{M}$  was estimated at pH 7. The obtained  
4  
5  
6  
7 CAC value for PA2 was 19  $\mu\text{M}$  at pH 7 (Figure 2D).  
8  
9

10 From these results, we decided to use WMR2PA as the antimicrobial moiety and both  
11  
12  
13  
14 PA1 and PA2 as inducers of the self-assembly process. We have thus focused our  
15  
16  
17 analysis on the two complexes PA1+WMR2PA and PA2+WMR2PA (Figure 2E and 2F).  
18  
19  
20  
21  
22  
23  
24



1  
2  
3  
4 **Figure 2.** The wavelength corresponding to the maximum fluorescence emission of Nile  
5  
6  
7 red was plotted as a function of concentration of the peptide WMR1PA (A), WMR2PA (B),  
8  
9  
10 PA1 (C), PA2 (D), and the complex PA1+WMR2PA (E) and PA2+WMR2PA (F) to  
11  
12  
13  
14 determine their CAC. The measurements were repeated three times.  
15  
16  
17  
18  
19  
20  
21

22 The mixture PA1+WMR2PA (50% mol/mol) shows a blue shift of Nile red indicating the  
23  
24  
25 ability to form aggregates (**Figure 2E**). The calculated CAC was 6  $\mu\text{M}$ , which is  
26  
27  
28 significantly lower than the one obtained for the peptide PA1 alone (16  $\mu\text{M}$ ). This is an  
29  
30  
31  
32 indication of the ability of PA1 to assist WMR2PA in the aggregation process.  
33  
34

35 The mixture PA2+WMR2PA (50% mol/mol) also shows the blue shift in the Nile red  
36  
37  
38  
39 emission at pH 7 and the calculated CAC is 4  $\mu\text{M}$ ; once again, we observe formation of  
40  
41  
42  
43 aggregates (**Figure 2F**).  
44  
45

46 **Table 2** summarized the CAC determined for individual peptides and mixtures.  
47  
48  
49 However, fluorescence provides the first glance at the formation of aggregates, but does  
50  
51  
52  
53  
54  
55  
56  
57  
58  
59  
60

not give any information about how the peptides interact to self-assemble or the morphology of the nanostructures formed. More characterizations were performed below.

<b>Table 2.</b> CAC ( $\mu\text{M}$ ) and zeta potential (mV) values determined for peptides and complexes						
	WMR1PA	WMR2PA	PA1	PA2	PA1+WMR2PA	PA2+WMR2PA
CAC	-	5	16	19	6	4
zeta potential		56.5	48.5	-37.9	37	34.8

### 3.2.2 Secondary structure

The molecular conformation of the peptides alone or in combination was investigated by far-UV CD spectroscopy, which is an excellent technique for rapid determination of the secondary structure and for studying the formation of peptide assemblies in solution (Figure 3). In fact, self-assembly is often accompanied by changes in secondary structures compared to monomers.

Concentration is a key parameter in controlling the self-assembly of peptides. At very low concentrations, peptides remain as monomers and start to aggregate above the CAC.

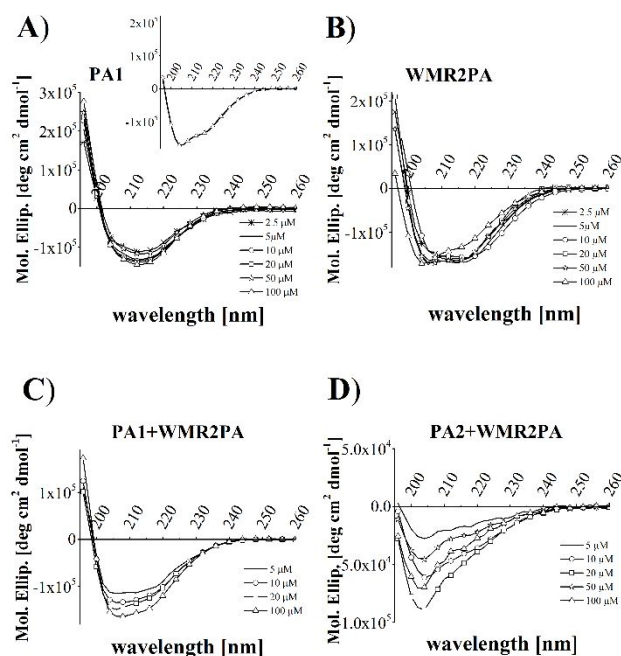


**Figure 3.** Conformation characterization of peptides PA1 (A) and WMR2PA (B), as well as peptide mixtures PA1+WMR2PA (C) and PA2+WMR2PA (D) by CD spectroscopy at different concentrations. The insert of the panel A is an enlargement of the spectra for the peptide PA1 at 100  $\mu\text{M}$ .

The spectrum of the peptide WMR2PA presents a large minimum in the region between 208 and 218 nm. This signal reveals a structure that falls into a non-canonical  $\alpha$ -helix or  $\beta$ -sheet conformation, but this pattern may be due to the co-existence of both structures.

1  
2  
3  
4 Nonetheless, the spectrum of the peptide WMR (from which WMR2PA was derived by  
5  
6  
7 addition of the moiety necessary for self-assembly) is a typical random coil conformation  
8  
9  
10 (data reported in a previous paper);<sup>30-31</sup> although the secondary structure of the WMR2PA  
11  
12  
13 monomer may also be different from that of WMR, these spectra were all reported at a  
14  
15  
16 concentration close/higher than the CAC, suggesting some sort of aggregations. It is  
17  
18  
19 interesting to note that at 100  $\mu$ M the spectrum obtained assumes features more typical  
20  
21  
22 of helical structures; we interpreted this as a proof of aggregation of WMR2PA at higher  
23  
24  
25 concentrations supported by the structuring in helical conformation and thus interaction  
26  
27  
28 among helices (Figure 3A, insert).  
29  
30  
31  
32  
33

34  
35 Also for peptide PA1, we observe a trend similar to the one of WMR2PA, which consists  
36  
37  
38 in a large band in the region between 208 and 218 nm.  
39  
40

41  
42 In contrast, the complexes PA1+WMR2PA and PA2+WMR2PA assume a conformation  
43  
44  
45 different from the ones adopted by the peptides alone. In the case of the mixture  
46  
47  
48 PA1+WMR2PA, the CD spectra show the presence of two minima resembling the typical  
49  
50  
51 minima of a helical structure. This characteristic is more evident for the complex  
52  
53  
54  
55  
56  
57  
58  
59  
60

1  
2  
3 PA2+WMR2PA. The CD spectra display the co-existence of  $\alpha$ -helix and  $\beta$ -sheet  
4  
5  
6  
7 structures with a predominance of the first one.  
8  
9

10 Raman spectroscopy is well recognized as a structure-specific analytical tool useful in  
11  
12  
13  
14 peptide analysis and was used here to characterize the peptides alone (**Figure 4A**) and  
15  
16  
17 their molecular interactions in the mixtures (**Figure 4B**). The peptides PA1 and WMR2PA  
18  
19  
20 have quite similar spectra, with few observable differences (if compared once normalized  
21  
22  
23 on the total area in the spectral range shown): the PA1 presents more intense bands at  
24  
25  
26  
27 1295 (Amide III region,  $\alpha$ -helix contribution), 1061 and 905  $\text{cm}^{-1}$  (C-C stretching modes).  
28  
29  
30 In the WMR2PA spectrum, the ratio of the bands at 880/841  $\text{cm}^{-1}$  (mainly contributed from  
31  
32  
33 Trp W17 and from Tyr Fermi doublets) is decreased and become below 1, possibly due  
34  
35  
36 to the Tyr residue being a strong donor of hydrogen bonds. The intensity ratio of the  
37  
38  
39 doublet at 757/724  $\text{cm}^{-1}$  (mainly contributed from Trp W18) is also decreased for  
40  
41  
42 WMR2PA compared to PA1. In contrast to PA1 and WMR2PA, the PA2 is void of aromatic  
43  
44  
45 amino acids: as the result, none of the Trp or Tyr bands described above are observed in  
46  
47  
48  
49 the spectrum of the PA2 peptide and the band at ca. 1550  $\text{cm}^{-1}$  (mainly contributed by  
50  
51  
52 Trp) is almost disappeared. In addition, the PA2 has a weaker band at 1436 ( $\text{CH}_2$   
53  
54  
55  
56  
57  
58  
59  
60

scissoring). This band is present in all the peptides, and contributed with the W6 mode of Trp when it is present.

The bands at 1236/1217  $\text{cm}^{-1}$  ( $\beta$ -sheet)<sup>49</sup> are relatively increased, while the band at 1295  $\text{cm}^{-1}$  ( $\alpha$ -helix) is higher than for WMR2PA. The C-C stretching bands of the PA2 are also different from those of PA1 and WMR2PA: stronger at 1093 and 905  $\text{cm}^{-1}$  and weaker at 1128  $\text{cm}^{-1}$ .

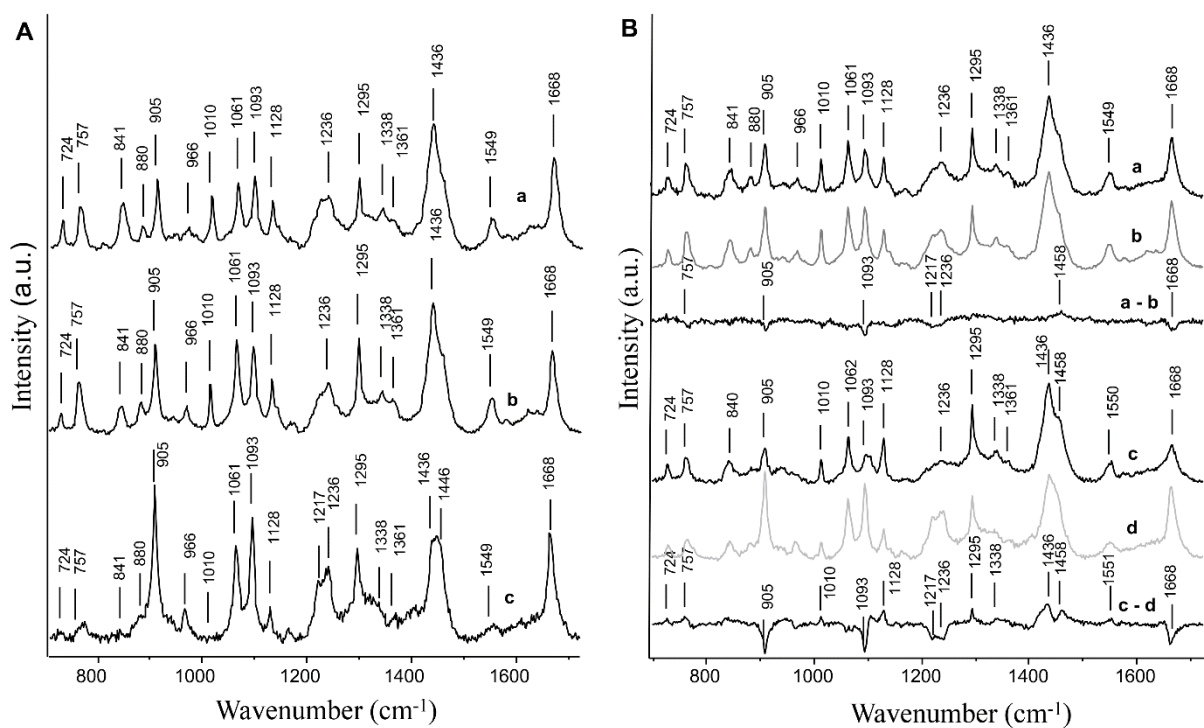


**Figure 4.** (A) Raman spectra of the peptides WMR2PA (a), PA1 (b) and PA2 (c). For better visual comparison, the spectra were normalized on the total intensity with the



1  
2  
3 shown spectral region. (B) Raman spectra of the binary complexes of the peptide  
4  
5  
6  
7 PA1&WMR2PA (a), PA2&WMR2PA (c), the sum of the respective peptides  
8  
9  
10 PA1+WMR2PA (b), and PA2+WMR2PA (d) and the respective difference spectra (A-B  
11  
12  
13  
14 and C-D).  
15  
16  
17  
18  
19  
20  
21

22 We analysed the spectra obtained for the PA1+WMR2PA and PA2+WMR2PA mixtures  
23  
24  
25 and compared them with those obtained from the sum of the spectra of the respective  
26  
27  
28 peptides, each normalized and taken at 50%. For the PA1+WMR2PA complex (**Figure**  
29  
30  
31 **4B, curve a**), the spectrum shape is very similar to that of the PA1+WMR2PA sum (**curve**  
32  
33  
34 **b**), the observed changes are weak but concern several bands: increase of the band at  
35  
36 1458  $\text{cm}^{-1}$  (CH and/or NH bending) and decrease of the bands at 1668 (antiparallel  $\beta$ -  
37  
38 sheet), 1236, 1217, 1093, 905 and 757  $\text{cm}^{-1}$  (C-C stretch). For the PA2+WMR2PA, the  
39  
40  
41 differences from the sum PA2+WMR2PA are more pronounced and concern even more  
42  
43  
44 bands. The decreased bands are the same as for the PA1+WMR2PA complex, except  
45  
46  
47 for the band at 757  $\text{cm}^{-1}$  that shows a weak increase. In addition, many bands are  
48  
49  
50  
51  
52  
53  
54  
55  
56  
57  
58  
59  
60

1  
2  
3 increased: at 1550 ( $\beta$ -sheet), 1436 ( $\text{CH}_2$  scissor), 1295 ( $\alpha$ -helix), 1128 (C-C stretch) and  
4  
5  
6  
7 1010 (C-C stretch, W18)  $\text{cm}^{-1}$ . These changes indicate that peptides underwent a  
8  
9  
10 conformational change upon interaction. These changes should be stronger in the  
11  
12  
13 PA2+WMR2PA complex, as indicated by the more pronounced spectral changes  
14  
15  
16  
17 observed.  
18  
19  
20

21 The position of the Trp band at 1010  $\text{cm}^{-1}$ , known as being sensitive to the strength of  
22  
23 van der Waals interactions of the Trp ring with surrounding residues, remains unchanged,  
24  
25  
26  
27 thus showing that these interactions were rather weak, in particular within the  
28  
29  
30  
31 PA2+WMR2PA complex.  
32  
33  
34

35 These data indicate that the tryptophan is probably not involved in the self-assembly  
36  
37  
38 process and the active moiety is more exposed and free to perform its activity.  
39  
40  
41

### 42 **3.2.3 Morphology of self-assembled nanostructures**

43  
44

45 To investigate the morphology of peptide assemblies, TEM imaging was carried out.  
46  
47  
48 The concentrations of the tested samples were 100 times higher than the CAC values  
49  
50  
51 and the pH was 7 for all the collected images. WMR2PA images show the formation of  
52  
53  
54  
55 nanostructures with the presence of numerous short fibres; we found a CAC of 5  $\mu\text{M}$  for  
56  
57  
58  
59  
60

WMR2PA (Figure 2B) indicating that the peptide is able to self-assemble. The design strategy was to reduce the content of the active sequence (the AMP sequence reported in green in Figure 1) and modulate its presence on the surface of the self-assembled nanosystem while retaining activity; thus, we were interested in the morphology attained for the complexes. We also analysed peptides PA1 (CAC 16  $\mu\text{M}$ ) and PA2 (CAC 19  $\mu\text{M}$ ), which bear respectively a positive and a negative charge, by TEM. For both, TEM shows that aggregation takes place with the formation of short belts for PA1 and short thin fibres for PA2 (Figure 5C and 5D).

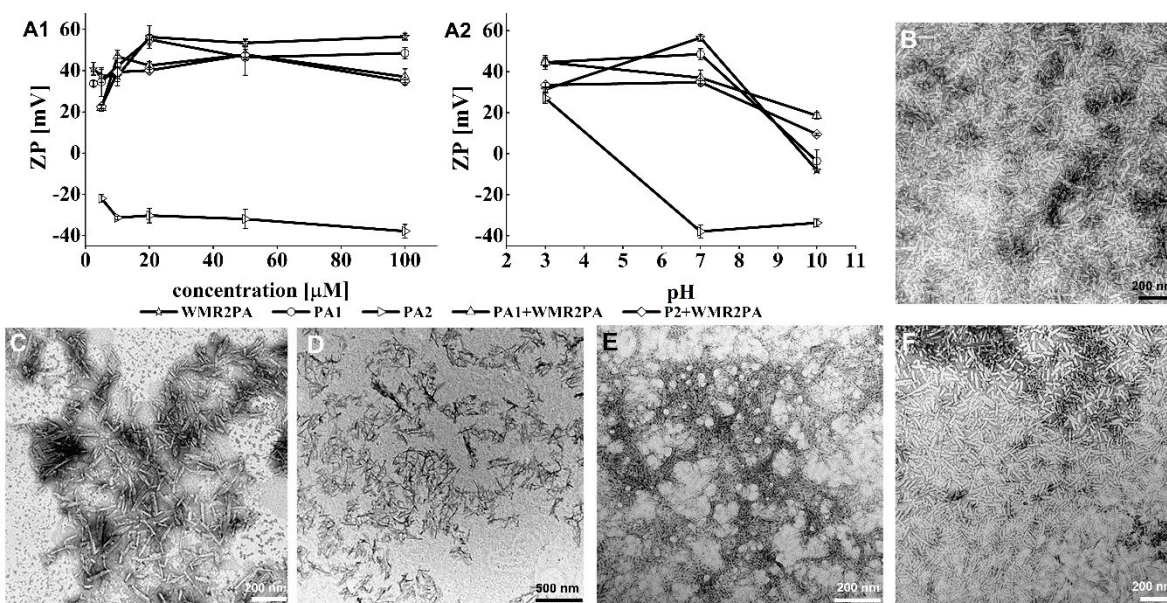


**Figure 5.** Zeta potential of the peptides measured at different concentrations and pHs (A).

Data are expressed as mean  $\pm$  standard deviations of three independent experiments.

1  
2  
3  
4 TEM images of nanostructures self-assembled from single peptide WMR2PA (B), PA1  
5  
6  
7 (C), and PA2 (D) and as well as peptide mixtures PA1+WMR2PA (E) and PA2+WMR2PA  
8  
9  
10 (F).

11  
12  
13  
14  
15  
16  
17  
18 When PA2 is mixed with WMR2PA (**Figure 5F**) we also observed short fibres very  
19  
20  
21 similar to the ones formed by WMR2PA alone (**Figure 5B**); while, when PA1 is mixed with  
22  
23  
24 WMR2PA (**Figure 5E**), we observe the formation of long fibres. The tryptophan may  
25  
26  
27 promote the elongation of the fibres, which are not arranged in a network; rather, they are  
28  
29  
30 intertwined in several entanglements. Moreover, at neutral pH the complexes  
31  
32  
33 PA1+WMR2PA and PA2+WMR2PA present distinct zeta-potential values (**Figure 5A**);  
34  
35  
36 thus, the difference in fibre length maybe not only due to the presence of tryptophan, but  
37  
38  
39 also the balance of electrostatic and hydrophobic forces among the molecules.  
40  
41  
42  
43  
44  
45

### 46 **3.2.4 Zeta-potential**

47  
48  
49 Analysis of the zeta-potential results clearly indicates that both peptides alone and  
50  
51  
52 complexes are stable under the conditions tested; in fact, the zeta-potential values are  
53  
54  
55  
56  
57  
58  
59  
60

1  
2  
3 typical of monodispersed preparations<sup>50</sup> (**Figure 5A1**). A positive zeta charge was  
4  
5  
6  
7 obtained for the peptides PA1 and WMR2PA, while a negative zeta charge was obtained  
8  
9  
10 for PA2, as expected. The TEM images (**Figure 5**) show that all three peptides are able  
11  
12  
13  
14 to assemble in nanostructures at pH 7.  
15

16  
17 The two complexes both showed positive zeta charges with a lower value for the  
18  
19  
20 complex PA2+WMR2PA. The CAC obtained for the complex PA2+WMR2PA is 4  $\mu$ M  
21  
22  
23 (**Figure 2F** and **Table 2**) and together with the zeta-potential values indicates the  
24  
25  
26  
27 formation of the complex, where the negative charges of PA2 are masked in the self-  
28  
29  
30 assembled structures.  
31  
32

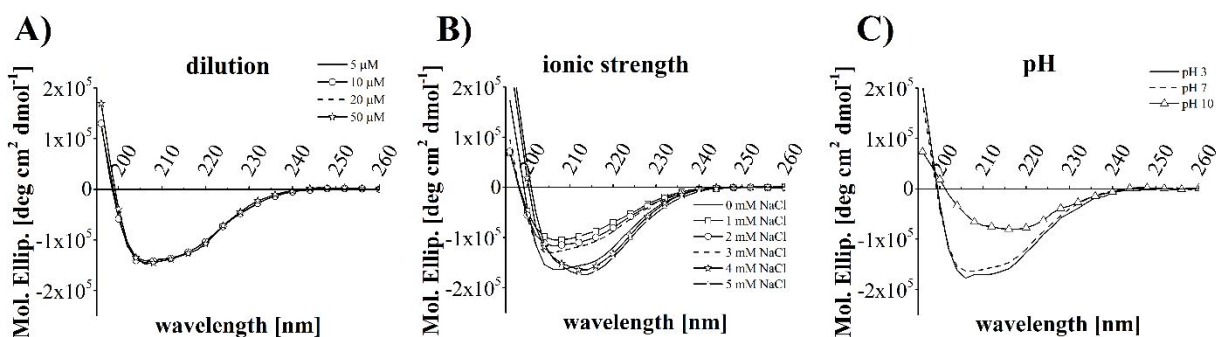
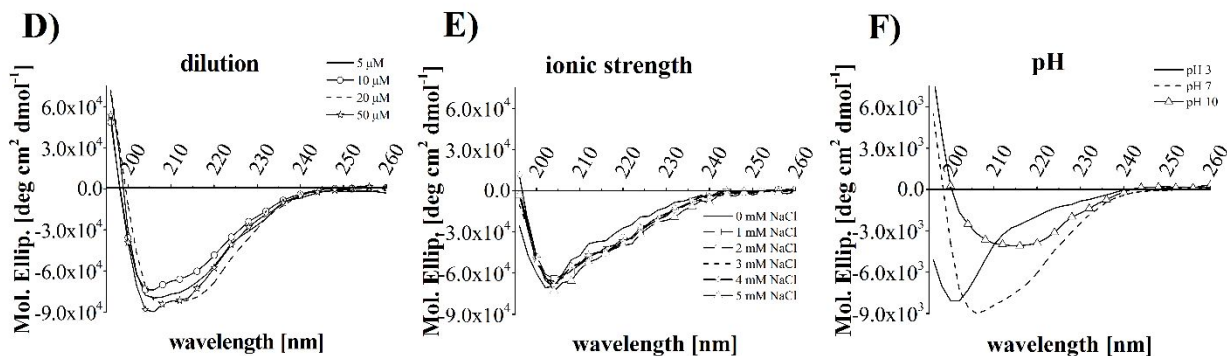
33  
34  
35 **Figure 5A2** reports the zeta-potential as a function of pH (pH 3, 7, 10). At pH 10, we  
36  
37  
38 observed a zeta-potential between 0 and 20 for all peptides (except PA2), which is  
39  
40  
41 indicative of a loss of charge in the self-assembled structures of isolated peptides and of  
42  
43  
44  
45 complexes.  
46  
47

### 48 49 **3.3 Effect of concentration, ionic strength and pH on peptide co-assemblies**

50

51  
52 In order to probe the effect of concentration, ionic strength and pH on the peptide co-  
53  
54  
55 assembly, circular dichroism spectra were collected at different conditions (**Figure 6**).  
56  
57  
58  
59  
60

1  
2  
3 Peptide samples were prepared at a total peptide concentration of 100  $\mu\text{M}$ . The solutions  
4  
5  
6  
7 were diluted with water and sonicated to break any type of pre-existing interactions; the  
8  
9  
10  
11 samples were lyophilized and rehydrated with the correct amount of solvent to achieve  
12  
13  
14 the desired concentration. Rehydration was performed only with water to probe the effect  
15  
16  
17 of dilution on the pre self-assembled structure, or with NaCl at different concentrations  
18  
19  
20 (from 0 to 5 mM NaCl) to probe the effect of the ionic strength and/or aqueous solution at  
21  
22  
23 different pHs.  
24  
25  
26  
27

**PA1 + WMR2PA****PA2 + WMR2PA**

1  
2  
3 **Figure 6.** CD spectra of the two complexes PA1+WMR2PA and PA2+WMR2PA upon  
4  
5  
6  
7 dilution (A, D) and at different ionic strengths (B, E) and pHs (C, F).  
8  
9

### 10 11 12 13 14 15 **3.3.1 Concentration** 16

17  
18 To analyse the effect of concentration on the structural stability of the assemblies, a  
19  
20 series of diluted solutions of the complexes were prepared and analysed by CD. We  
21  
22 examined the concentration effect on the stability of the self-assembled structures of  
23  
24 PA1+WMR2PA and PA2+WMR2PA (**Figure 6A and 6D**). For both complexes, the spectra  
25  
26 are completely overlapped even near the CAC value, indicating the absence of any  
27  
28 perturbation on the packing of pre-formed self-assembled nanofibers upon dilution, and  
29  
30 also indicating stability of the aggregates. Analysing the dilution effect is fundamental, in  
31  
32 particular for the biological tests, where the self-assembled structures are prepared at  
33  
34 concentration well above the CAC, but then diluted.  
35  
36  
37  
38  
39  
40  
41  
42  
43  
44  
45  
46  
47  
48

### 49 **3.3.2 Ionic strength** 50 51 52 53 54 55 56 57 58 59 60

1  
2  
3  
4 Given the presence of salts in body fluids, we evaluated the effect of ionic strength on  
5  
6  
7 the aggregate stability (**Figure 6B** and **6E**). The complex PA2+WMR2PA shows the same  
8  
9  
10 conformational features of the ones in pure water, indicating stability of the assemblies  
11  
12  
13 even in the presence of salts. In contrast, CD spectra of the complex PA1+WMR2PA  
14  
15  
16 showed a signal with a predominant  $\beta$ -sheet contribution at 4 mM and 5 mM NaCl,  
17  
18  
19 presumably due to the interactions between the peptides and the salt ions. Increasing  
20  
21  
22 concentrations of NaCl could effectively promote the  $\beta$ -sheet conformation when charges  
23  
24  
25 of the lysine side chains are screened by  $\text{Cl}^-$  ions and thus favour the packing of  
26  
27  
28 molecules, as also reported in literature.<sup>12</sup> This is evident on the complex PA1+WMR2PA,  
29  
30  
31 in which the positive charges of lysines are not balanced by negative charges of the  
32  
33  
34 aspartic acid present in the complex PA2+WMR2PA.  
35  
36  
37  
38  
39  
40

### 41 **3.3.3 pH**

42  
43  
44  
45 The effect of pH on the stability of the self-assembled peptide nanostructures was  
46  
47  
48 analysed by CD at a total peptide concentration of 100  $\mu\text{M}$  (**Figure 6C** and **6F**). For the  
49  
50  
51 PA1+WMR2PA complex, we observed a very similar behaviour at pH 3 and 7, while at  
52  
53  
54 pH 10 the nanostructures assume a secondary conformation (probably  $\beta$ -sheet), due to  
55  
56  
57  
58  
59  
60



1  
2  
3 the reduced positive net charge, which may favour stronger interactions between  
4  
5  
6  
7 peptides.  
8  
9

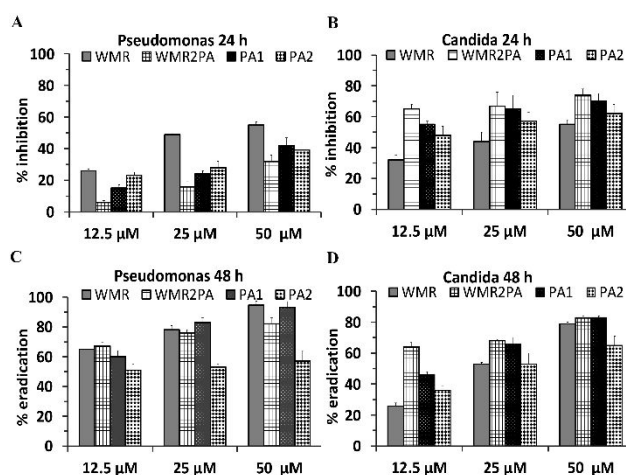
10 The pKa of the lysine side chain is 10.5 and that of the arginine side chain is 12.5. The  
11  
12  
13 complex PA1+WMR2PA presents a total of four arginine and three lysine residues. Thus,  
14  
15  
16 when the pH is below 10, the two peptides have a total charge of +7 which prevents the  
17  
18  
19  
20  
21 flanking sequences from approaching each other and hinders their self-assembly. The  
22  
23  
24 spectra at pH 3 and pH 7 are similar and indicative of a helical structure. At pH 10, the  
25  
26  
27 majority of the amine groups are unprotonated (neutral, as confirmed by the zeta-potential  
28  
29  
30  
31 measurements, **Figure 5A**) favouring peptide aggregation, as shown by a  $\beta$ -sheet signal  
32  
33  
34 in the CD spectrum. The aggregated form may also be attributed to formation of coiled  
35  
36  
37  
38 coil structures; in fact, the ratio of ellipticities at 222 nm and 208 nm, can be used to  
39  
40  
41 distinguish between monomeric and oligomeric states of helices.<sup>51</sup> When the ratio  
42  
43  
44  $\theta_{222}/\theta_{208}$  equals about 0.8, the peptide is monomeric, and when the ratio exceeds 1.0 it is  
45  
46  
47 oligomeric. In our case, we have for PA2+WMR2PA a ratio of 0.2 (pH3), 0.6 (pH 7) and  
48  
49  
50  
51  
52 1.0 (pH10), indicating aggregation as a function of pH.  
53  
54  
55  
56  
57  
58  
59  
60

The complex PA2+WMR2PA contains three arginines, two lysines and two aspartic acids, with a total net charge of +3. We observe a different behaviour in this complex compared to PA1+WMR2PA, with a different spectrum at each pH (3, 7, and 10). In particular, the peptides started to aggregate at pH 7 with complete aggregation at pH 10.

The data obtained clearly show that the electrostatic interactions play a key role in controlling the nanofiber formation and stability, governing also the disassembly in aqueous solutions.

### 3.4 Anti-biofilm activity of the self-assembled peptides

To assess the potential of the self-assembled nanostructures to inhibit the formation or to eradicate the pre-formed biofilms, biofilms of two representative species, the Gram-negative bacterium *P. aeruginosa* and the fungus *C. albicans* were used.



1  
2  
3 **Figure 7.** Effect of peptides WMR, WMR2PA, PA1, and PA2 on *Pseudomonas* and  
4  
5  
6  
7 *Candida* biofilms to evaluate both inhibition (A, B) and eradication (C, D) conditions.  
8  
9

10  
11  
12  
13  
14  
15 The activity of the sequence WMR against *P. aeruginosa* in planktonic cells was  
16  
17  
18 previously reported (MIC 2  $\mu\text{M}$ ).<sup>30-31</sup> The activity of WMR against biofilms of both *P.*  
19  
20  
21 *aeruginosa* and *C. albicans* was first tested here. WMR shows less activity against *P.*  
22  
23  
24 *aeruginosa* biofilm compared to planktonic cells. At the lowest concentration tested (12.5  
25  
26  
27  $\mu\text{M}$ ), a 20% inhibition was obtained at 24 h of biofilm formation (**Figure 7A**), while at the  
28  
29  
30 same concentration, complete inhibition of *P. aeruginosa* planktonic cell growth was  
31  
32  
33 achieved.<sup>30-31</sup> Interestingly, the activity against a 48 h *P. aeruginosa* biofilm was  
34  
35  
36 enhanced indicating that the peptide is able to eradicate the pre-formed biofilm (**Figure**  
37  
38  
39 **7C**). At the same concentration, WMR presents a lower ability to inhibit and eradicate  
40  
41  
42 *Candida* biofilms (**Figure 7B** and **7D**). Nonetheless, both biofilms were impaired at 48 h  
43  
44  
45 when using high concentrations (50  $\mu\text{M}$ ) of WMR. The next step was to compare the  
46  
47  
48 activity of WMR (the native sequence) with that of WMR2PA (which corresponds to WMR  
49  
50  
51  
52  
53  
54  
55  
56  
57  
58  
59  
60

1  
2  
3 modified at the C-terminus with alanines and a hydrophobic tail). The results indicate a  
4  
5  
6  
7 loss of activity (concentration-dependent) against *P. aeruginosa* biofilms at 24 h (**Figure**  
8  
9  
10 **7A**), whereas an enhanced activity against the *C. albicans* biofilms at 24 h was observed  
11  
12  
13 (**Figure 7B**). Furthermore, we analysed the effect of P1 and P2, which contain the  
14  
15  
16 hydrophobic tail but not the AMP sequence. Surprisingly, we observed recovered activity  
17  
18  
19 against *P. aeruginosa* at 24 h and enhanced activity in all other conditions. The analysis  
20  
21  
22 of the results show that the hydrophobic tail plays a key role in both inhibition and  
23  
24  
25 eradication of *Candida* biofilms, while its role is milder in the inhibition of *Pseudomonas*  
26  
27  
28 biofilms, where we observed higher activity for WMR compared to PA sequences.  
29  
30  
31  
32  
33  
34  
35 Analysis of the data from the literature on the composition of the outer bacterial (*P.*  
36  
37  
38 *aeruginosa*) and fungal (*C. albicans*) membrane, revealed that both are negatively  
39  
40  
41 charged but the fungal membrane contains a sterol (ergosterol).<sup>52-53</sup> WMR2PA and PA1  
42  
43  
44 are positively charged while PA2 is negatively charged and they are all aggregated in the  
45  
46  
47 condition tested. The charge, while being a key parameter to inhibit *P. aeruginosa* biofilm  
48  
49  
50 preventing the initial adhesion of the bacteria (which has a negatively charged surface),  
51  
52  
53 may not be the critical parameter in eradication of both biofilms and in the inhibition of *C.*  
54  
55  
56  
57  
58  
59  
60

1  
2  
3  
4 *albicans*; where a prominent role is played by the hydrophobic tail. PA2 has a net negative  
5  
6  
7 charge as the outer membrane of Gram-negative bacteria; thus, we hypothesize that the  
8  
9  
10 lipid chain is mainly involved in the interaction with lipids and maybe with the other non-  
11  
12  
13  
14 lipidic components of the outer membrane which may determine its mechanism of activity.  
15

16  
17 The role of the C19 in *C. albicans* biofilm may be correlated to the putative interaction  
18  
19  
20 with ergosterol. Indeed, the eukaryotic membranes, apart from being zwitterionic, also  
21  
22  
23  
24 contain a sterol (cholesterol), but we do not observe toxicity (see next paragraph) at the  
25  
26  
27  
28 concentration used. Fungal and eukaryotic membranes differ with respect to sterol  
29  
30  
31 identity. Although being structurally similar, their effects on membranes physical  
32  
33  
34 parameters are different<sup>52-53</sup> with cholesterol increasing lipid order while maintaining  
35  
36  
37  
38 fluidity; the presence of tryptophan residues is also critical because this residue is usually  
39  
40  
41  
42 located close to the interface between aqueous solutions and membranes, but due to its  
43  
44  
45 bulky nature it is sensitive to sterol identity as reported for other AMPs with antifungal  
46  
47  
48 activity and low toxicity for epithelial cells.<sup>54</sup> Thus, we speculated that the C19 tail and the  
49  
50  
51  
52 tryptophan are both responsible for the interaction with the ergosterol, which favours their  
53  
54  
55  
56 antibacterial and antifungal activity, as well as their low toxicity.  
57  
58  
59  
60

1  
2  
3  
4 **Figure 8** reports the data obtained for the two complexes PA1+WMR2PA and  
5  
6  
7 PA2+WMR2PA, in comparison to WMR (the native monomeric sequence). The CACs for  
8  
9  
10 the two complexes are 6 and 4  $\mu\text{M}$ , respectively, and the complexes once formed are  
11  
12  
13 able to withstand dilution effects; thus, in the condition tested they are self-assembled  
14  
15  
16  
17 (**Figure 2**). Both complexes PA1+WMR2PA and PA2+WMR2PA were active against  
18  
19  
20  
21 *Candida* biofilms at 24 and 48 h (**Figure 8B and D**), indicating that they were both effective  
22  
23  
24 for biofilm prevention and eradication and they show enhanced activity compared to  
25  
26  
27 WMR. On the contrary, we observe comparable activity to WMR for inhibition and  
28  
29  
30  
31 eradication of *Pseudomonas* biofilm (**Figure 8A and C**).  
32  
33  
34  
35  
36  
37  
38  
39  
40  
41  
42  
43  
44  
45  
46  
47  
48  
49  
50  
51  
52  
53  
54  
55  
56  
57  
58  
59  
60

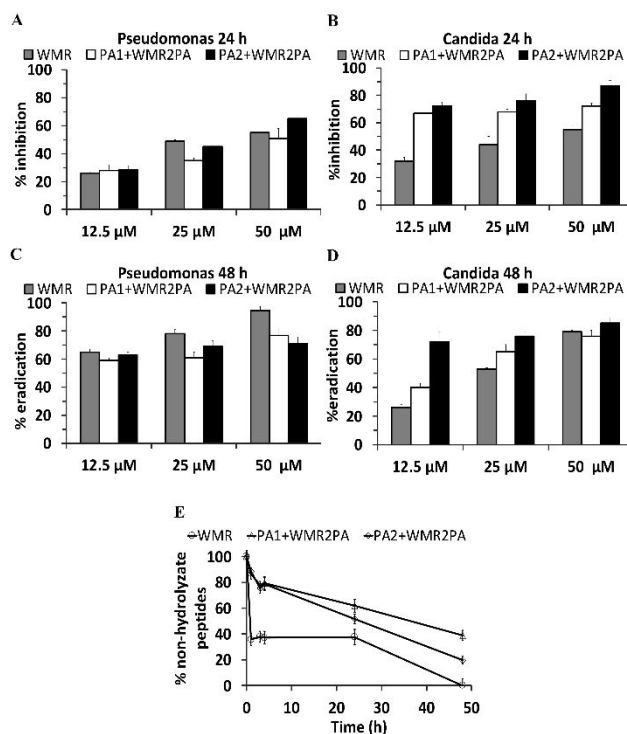


**Figure 8.** Effect of peptides WMR and complexes PA1+WMR2PA and PA2+WMR2PA on *Pseudomonas* and *Candida* biofilms to evaluate both inhibition (A, B) and eradication conditions (C, D). Proteolytic stability of WMR and complexes PA1+WMR2PA and PA2+WMR2PA monitored by analytical-HPLC at different incubation times with trypsin (E).

The nanofibers co-assembled from the designed peptides not only inhibit the biofilm formation but also eradicate the pre-formed biofilms, which have been both considered

1  
2  
3 as key processes for applications in antimicrobial therapies. It is likely that prevention of  
4  
5  
6  
7 biofilm growth may be related to killing of planktonic bacteria prior to attachment, and for  
8  
9  
10 inhibiting adhesion of bacteria, critical initial steps in biofilm formation, which may be  
11  
12  
13 attributed not only to the AMP sequence but also to the presence of the hydrophobic tail,  
14  
15  
16 which disturbs the formation of the biofilm matrix. Many AMPs are more effective in  
17  
18  
19 inhibiting the early phases of biofilm development rather than in eradicating established  
20  
21  
22 biofilms.<sup>3</sup> On the contrary, the co-assembled nanofibers have shown a strong ability also  
23  
24  
25  
26 to eradicate pre-formed biofilms which may be attributed to their ability to disaggregate  
27  
28  
29 the matrix of pre-formed biofilms, and diffuse into the deep layers of the biofilm killing  
30  
31  
32 bacteria inside the biofilm.<sup>3</sup> Overall, these results indicate that a possible mechanism of  
33  
34  
35 anti-biofilm activity may be related to a “non-classical” mode of action which does not  
36  
37  
38 involve only the microbicide effect, but also interference with specific targets of the biofilm  
39  
40  
41 lifestyle, such as extracellular matrix production and assembly, and it will be worth to  
42  
43  
44 verify whether it is also capable of influencing microorganism cell-to-cell communication  
45  
46  
47 and intracellular signalling systems.<sup>3</sup>  
48  
49  
50  
51  
52  
53  
54  
55  
56  
57  
58  
59  
60



1  
2  
3 The data reported show that both the peptide complexes possess enhanced activity  
4 compared to WMR against *Candida* biofilms but a similar activity against *Pseudomonas*  
5  
6  
7 biofilm. Although we were unable to enhance activity against *P. aeruginosa* biofilms, we  
8  
9  
10 were still able to achieve active complexes and the benefit is represented by their  
11  
12  
13 enhanced proteolytic resistance (**Figure 8E**), which is an added value for therapeutic  
14  
15  
16 applications.  
17  
18  
19  
20  
21  
22  
23

### 24 **3.5 Proteolytic stability**

25  
26  
27 A significant limitation of peptides as therapeutics is their susceptibility to protease  
28  
29  
30 degradation. The proteolytic stability of the self-assembled peptide nanostructures was  
31  
32  
33 evaluated by incubation with a common protease enzyme, trypsin, for 48 h and the  
34  
35  
36 degradation process was monitored by RP-HPLC. As expected, the native AMP  
37  
38  
39 sequence, WMR, was rapidly hydrolysed by trypsin into two peptide fragments after 1 h  
40  
41  
42 (**Figure 8E and S1**). Chemical modifications of the sequence and formation of self-  
43  
44  
45 assembled structures can significantly reduce the enzymatic degradation rate. Both  
46  
47  
48 peptide complexes PA1+WMR2PA and PA2+WMR2PA remained stable up to 4 h (**Figure**  
49  
50  
51  
52  
53  
54  
55  
56  
57  
58  
59  
60 **8E and S1**). Partial degradations at 24 and 48 h were observed, but a significant part of

1  
2  
3 the active peptide was still present as shown in **Figure 8E**. After 48 h, we still observe the  
4  
5  
6  
7 presence of peak corresponding to the peptide (approximately 50%). Clearly, the  
8  
9  
10 addition of the hydrophobic tail in WMR2PA and the formation of supramolecular  
11  
12  
13  
14 assemblies can be used as a viable strategy to improve the protease susceptibilities of  
15  
16  
17 antimicrobial peptides.  
18

### 21 **3.6 Biocompatibility and selectivity**

22  
23  
24 The selective interaction with bacterial cells, the cytotoxicity towards human cells, as  
25  
26  
27 well as the haemolytic activity of the self-assembled peptide nanostructures were  
28  
29  
30  
31 evaluated. The results (**Figure 9**) clearly demonstrate that the self-assembled peptide  
32  
33  
34 nanostructures are selective for bacterial cells and are nontoxic for human cells.  
35

36  
37  
38 We found low cytotoxicity of the peptide nanostructures on Vero cells even at higher  
39  
40  
41 concentration (200  $\mu\text{M}$ ) both at 1 and 24 h post exposure (**Figure 9A** and **9B**). Maximum  
42  
43  
44 cell toxicity (60%) was observed for WMR2PA at 200  $\mu\text{M}$  after 24 h. However, WMR2PA  
45  
46  
47 is already active against the tested pathogens at lower concentrations, at which the  
48  
49  
50  
51 peptide does not show toxicity to mammalian cells. Furthermore, WMR2PA was co-  
52  
53  
54  
55 assembled with PA1 or PA2, which were clearly non-toxic.  
56  
57  
58  
59  
60

In the evaluation of the haemolytic activity, only WMR2PA shows a partial toxic effect (Figure 9C). This toxicity (less than 50%) was maintained when WMR2PA is associated with the peptides PA1 and PA2. Nevertheless, this toxicity is observed only at higher concentrations, leading to the fact that these peptides present low toxicity and low haemolytic activity at the concentrations used to prepare the nanostructures and for the anti-biofilm assays.

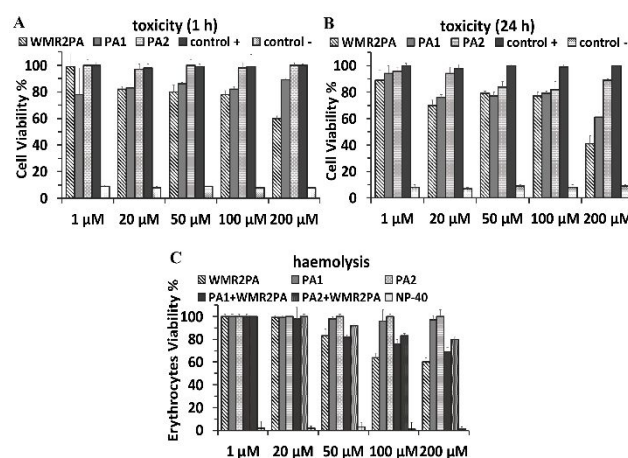


**Figure 9.** Effect of peptides WMR, PA1, WMR2PA, PA2 and complexes PA1+WMR2PA and PA2+WMR2PA on Vero cells at 1 h (A) and 24 h (B), as well as red blood cells (C) to evaluate their biocompatibility.

#### 4 Conclusion

1  
2  
3  
4 In this study, a proof of concept is provided showing how nanoscale engineering can  
5  
6  
7 be exploited to produce supramolecular peptide-based platforms with potent antibacterial  
8  
9  
10 activity, improved functionalities, as well as enhanced biocompatibility compared to other  
11  
12  
13 antimicrobial agents. These supramolecular peptide-based nanotechnology could serve  
14  
15  
16 as an important class of antibacterial compounds for the treatment of intracellular  
17  
18  
19 microbial infections.<sup>54</sup>  
20  
21  
22  
23

24 Novel methods for effective biofilm inhibition and/or eradication are very much needed  
25  
26  
27 to prevent infection and consequent rejection of implantable biomaterials. Self-assembly  
28  
29  
30 was used here for the multivalent presentation of a known AMP onto defined  
31  
32  
33 nanostructures. The presence of AMP sequence on the periphery of the self-assembled  
34  
35  
36 nanofibers increases its effective local concentration, compared to soluble peptides, and  
37  
38  
39 enhances the overall antibacterial activity. The anti-biofilm activity is also enhanced under  
40  
41  
42 the nanofiber configuration compared to soluble peptides. Moreover, the self-assembled  
43  
44  
45 nanostructures can also provide a mean to increase its stability and half-life, which is one  
46  
47  
48 limitation of peptide therapeutics compared with most other antibiotics. To improve the  
49  
50  
51 anti-biofilm properties, current focus of research is to combine the designed  
52  
53  
54  
55  
56  
57  
58  
59  
60

1  
2  
3 nanostructures with conventional antibiotics. The synergistic combinations have the  
4  
5  
6  
7 potential to decrease the effective concentration of the active molecules, as well as to  
8  
9  
10 extend their spectrum of action, thereby reducing the spread of resistance, which is often  
11  
12  
13 linked to monotherapy regimens. The use of self-assembled nanomaterials described in  
14  
15  
16  
17 this work may also allow the integration of other AMPs without compromising the  
18  
19  
20  
21 nanostructure for the development of novel antibacterial materials.  
22  
23  
24  
25  
26  
27  
28

## 29 ASSOCIATED CONTENT

30  
31  
32  
33 **Supporting information** Supporting information: Comparison of enzymatic resistance of  
34  
35  
36 the antimicrobial peptide WMR alone and in self-assembling fibers (PA1+WMR2PA,  
37  
38  
39 PA2+WMR2PA) monitored by HPLC at different time: 1, 3, 4, 24 and 48 hours.  
40  
41  
42  
43  
44

## 45 AUTHOR INFORMATION

### 46 47 48 **Corresponding Author**

49  
50  
51  
52 \* Stefania Galdiero, stefania.galdiero@unina.it  
53  
54  
55  
56  
57  
58  
59  
60

## Author Contributions

The manuscript was written through contributions of all authors. All authors have given approval to the final version of the manuscript.

## Funding Sources

Y. Shi and H. S. Azevedo grateful acknowledge the Seed Award in Science (grant reference number: 210122/Z/18/Z) granted by the Wellcome Trust. S. Galdiero grateful acknowledges the POR CAMPANIA FESR 2014/2020 “Progetto premio infrastruttura per la medicina di precisione in oncologia”

## Conflicts of interest

There are no conflicts to declare.

## REFERENCES

- (1) Falanga, A.; Galdiero, S., Emerging therapeutic agents on the basis of naturally occurring antimicrobial peptides. In *Amino Acids, Peptides and Proteins: Volume 42*, The Royal Society of Chemistry: 2018; Vol. 42, pp 190-227.
- (2) Riool, M.; de Breij, A.; Drijfhout, J. W.; Nibbering, P. H.; Zaat, S. A. J., Antimicrobial Peptides in Biomedical Device Manufacturing. *Front. Chem.* **2017**, *5*, 63.
- (3) Delattin, N.; De Brucker, K.; De Cremer, K.; Cammue, B. P. A.; Thevissen, K., Antimicrobial Peptides as a Strategy to Combat Fungal Biofilms. *Curr. Top. Med. Chem.* **2017**, *17*(5), 604-612.
- (4) Mendes, A. C.; Baran, E. T.; Reis, R. L.; Azevedo, H. S., Self-assembly in nature: using the principles of nature to create complex nanobiomaterials. *Wiley Interdiscip. Rev.: Nanomed. Nanobiotechnol.* **2013**, *5*(6), 582-612.
- (5) Rad-Malekshahi, M.; Lempsink, L.; Amidi, M.; Hennink, W. E.; Mastrobattista, E., Biomedical Applications of Self-Assembling Peptides. *Bioconjugate Chem.* **2016**, *27*(1), 3-18.
- (6) McCloskey, A.; Gilmore, B.; Laverty, G., Evolution of Antimicrobial Peptides to Self-Assembled Peptides for Biomaterial Applications. *Pathogens* **2014**, *3*(4), 791-821.
- (7) Alves, D.; Olívia Pereira, M., Mini-review: Antimicrobial peptides and enzymes as promising candidates to functionalize biomaterial surfaces. *Biofouling* **2014**, *30*(4), 483-499.
- (8) Galdiero, S.; Falanga, A.; Berisio, R.; Grieco, P.; Morelli, G.; Galdiero, M., Antimicrobial peptides as an opportunity against bacterial diseases. *Curr. Med. Chem.* **2015**, *22*(14), 1665-1677.
- (9) Scudiero, O.; Nigro, E.; Cantisani, M.; Colavita, I.; Leone, M.; Mercurio, F. A.; Galdiero, M.; Pessi, A.; Daniele, A.; Salvatore, F.; Galdiero, S., Design and activity of a cyclic mini- $\beta$ -defensin analog: a novel antimicrobial tool. *Int. J. Nanomed.* **2015**, *10*, 6523-6539.
- (10) Scudiero, O.; Galdiero, S.; Nigro, E.; Del Vecchio, L.; Di Noto, R.; Cantisani, M.; Colavita, I.; Galdiero, M.; Cassiman, J. J.; Daniele, A.; Pedone, C.; Salvatore, F., Chimeric beta-defensin analogs, including the novel 3NI analog, display salt-resistant

- 1  
2  
3 antimicrobial activity and lack toxicity in human epithelial cell lines. *Antimicrob. Agents*  
4 *Chemother.* **2013**, *57*(4), 1701-1708.
- 5  
6  
7 (11) Scudiero, O.; Galdiero, S.; Cantisani, M.; Di Noto, R.; Vitiello, M.; Galdiero, M.;  
8 Naclerio, G.; Cassiman, J. J.; Pedone, C.; Castaldo, G.; Salvatore, F., Novel synthetic,  
9 salt-resistant analogs of human beta-defensins 1 and 3 endowed with enhanced  
10 antimicrobial activity. *Antimicrob. Agents Chemother.* **2010**, *54*(6), 2312-2322.
- 11  
12  
13 (12) Liu, Y.; Yang, Y.; Wang, C.; Zhao, X., Stimuli-responsive self-assembling  
14 peptides made from antibacterial peptides. *Nanoscale* **2013**, *5*(14), 6413-6421.
- 15  
16  
17 (13) McCloskey, A. P.; Draper, E. R.; Gilmore, B. F.; Laverty, G., Ultrashort self-  
18 assembling Fmoc-peptide gelators for anti-infective biomaterial applications. *J. Pept.*  
19 *Sci.* **2017**, *23*(2), 131-140.
- 20  
21  
22 (14) Laverty, G.; McCloskey, A. P.; Gilmore, B. F.; Jones, D. S.; Zhou, J.; Xu, B.,  
23 Ultrashort Cationic Naphthalene-Derived Self-Assembled Peptides as Antimicrobial  
24 Nanomaterials. *Biomacromolecules* **2014**, *15*(9), 3429-3439.
- 25  
26  
27 (15) Schnaider, L.; Brahmachari, S.; Schmidt, N. W.; Mensa, B.; Shaham-Niv, S.;  
28 Bychenko, D.; Adler-Abramovich, L.; Shimon, L. J. W.; Kolusheva, S.; DeGrado, W. F.;  
29 Gazit, E., Self-assembling dipeptide antibacterial nanostructures with membrane  
30 disrupting activity. *Nat. Commun.* **2017**, *8*(1), 1365-1375.
- 31  
32  
33 (16) Beter, M.; Kara, H. K.; Topal, A. E.; Dana, A.; Tekinay, A. B.; Guler, M. O.,  
34 Multivalent Presentation of Cationic Peptides on Supramolecular Nanofibers for  
35 Antimicrobial Activity. *Mol. Pharmaceutics* **2017**, *14*(11), 3660-3668.
- 36  
37  
38 (17) Tian, X.; Sun, F.; Zhou, X. R.; Luo, S. Z.; Chen, L., Role of peptide self-assembly  
39 in antimicrobial peptides. *J. Pept. Sci.* **2015**, *21*(7), 530-539.
- 40  
41  
42 (18) Mitra, R. N.; Shome, A.; Paul, P.; Das, P. K., Antimicrobial activity,  
43 biocompatibility and hydrogelation ability of dipeptide-based amphiphiles. *Org. Biomol.*  
44 *Chem.* **2009**, *7*(1), 94-102.
- 45  
46  
47 (19) Chen, C.; Hu, J.; Zhang, S.; Zhou, P.; Zhao, X.; Xu, H.; Zhao, X.; Yaseen, M.; Lu,  
48 J. R., Molecular mechanisms of antibacterial and antitumor actions of designed  
49 surfactant-like peptides. *Biomaterials* **2012**, *33*(2), 592-603.
- 50  
51  
52 (20) Hendricks, M. P.; Sato, K.; Palmer, L. C.; Stupp, S. I., Supramolecular Assembly  
53 of Peptide Amphiphiles. *Acc. Chem. Res.* **2017**, *50*(10), 2440-2448.
- 54  
55  
56  
57  
58  
59  
60



- 1  
2  
3  
4 (21) Dooling, L. J.; Tirrell, D. A., Engineering the Dynamic Properties of Protein  
5 Networks through Sequence Variation. *ACS Cent. Sci.* **2016**, *2*(11), 812-819.  
6  
7 (22) Welsh, E. R.; Tirrell, D. A., Engineering the extracellular matrix: a novel approach  
8 to polymeric biomaterials. I. Control of the physical properties of artificial protein  
9 matrices designed to support adhesion of vascular endothelial cells. *Biomacromolecules*  
10 **2000**, *1*(1), 23-30.  
11  
12 (23) Zhang, S., Discovery and design of self-assembling peptides. *Interface Focus*  
13 **2017**, *7*(6).  
14  
15 (24) Vauthey, S.; Santoso, S.; Gong, H.; Watson, N.; Zhang, S., Molecular self-  
16 assembly of surfactant-like peptides to form nanotubes and nanovesicles. *Proc. Natl.*  
17 *Acad. Sci. U. S. A.* **2002**, *99*(8), 5355-5360.  
18  
19 (25) Sun, Y.; Wollenberg, A. L.; O'Shea, T. M.; Cui, Y.; Zhou, Z. H.; Sofroniew, M. V.;  
20 Deming, T. J., Conformation-Directed Formation of Self-Healing Diblock Copolypeptide  
21 Hydrogels via Polyion Complexation. *J. Am. Chem. Soc.* **2017**, *139*(42), 15114-15121.  
22  
23 (26) Nowak, A. P.; Breedveld, V.; Pakstis, L.; Ozbas, B.; Pine, D. J.; Pochan, D.;  
24 Deming, T. J., Rapidly recovering hydrogel scaffolds from self-assembling diblock  
25 copolypeptide amphiphiles. *Nature* **2002**, *417*(6887), 424-428.  
26  
27 (27) Hamley, I. W. D., A.; Castelletto, V.; Furzeland, S.; Atkins, D.; Seitsonen, J.;  
28 Ruokolainen, J., Reversible helical unwinding transition of a self-assembling peptide  
29 amphiphile. *Soft Matter* **2013**, *9*, 9290-9293.  
30  
31 (28) Hamley, I. W.; Castelletto, V., Self-Assembly of Peptide Bioconjugates: Selected  
32 Recent Research Highlights. *Bioconjugate Chem.* **2017**, *28*(3), 731-739.  
33  
34 (29) Ekiz, M. S.; Cinar, G.; Khalily, M. A.; Guler, M. O., Self-assembled peptide  
35 nanostructures for functional materials. *Nanotechnology* **2016**, *27*(40), 402002-402039.  
36  
37 (30) Cantisani, M.; Finamore, E.; Mignogna, E.; Falanga, A.; Nicoletti, G. F.; Pedone,  
38 C.; Morelli, G.; Leone, M.; Galdiero, M.; Galdiero, S., Structural Insights into and Activity  
39 Analysis of the Antimicrobial Peptide Myxinidin. *Antimicrob. Agents Chemother.* **2014**,  
40 *58*(9), 5280-5290.  
41  
42 (31) Cantisani, M.; Leone, M.; Mignogna, E.; Kampanaraki, K.; Falanga, A.; Morelli,  
43 G.; Galdiero, M.; Galdiero, S., Structure activity relations of myxinidin, an antibacterial  
44  
45  
46  
47  
48  
49  
50  
51  
52  
53  
54  
55  
56  
57  
58  
59  
60

1  
2  
3 peptide derived from Epidermal Mucus of Hagfish. *Antimicrob. Agents Chemother.*  
4 **2013**, *57*(11), 5665-5673.

5  
6  
7 (32) Lombardi, L.; Stellato, M. I.; Oliva, R.; Falanga, A.; Galdiero, M.; Petraccone, L.;  
8 D'Errico, G.; De Santis, A.; Galdiero, S.; Del Vecchio, P., Antimicrobial peptides at work:  
9 interaction of myxinidin and its mutant WMR with lipid bilayers mimicking the P.  
10 *aeruginosa* and *E. coli* membranes. *Sci. Rep.* **2017**, *7*, 44425-44440.

11  
12 (33) Subramanian, S.; Ross, N. W.; Mackinnon, S. L., Comparison of the biochemical  
13 composition of normal epidermal mucus and extruded slime of hagfish (*Myxine*  
14 *glutinosa* L.). *Fish Shellfish Immunol.* **2008**, *25*(5), 625-632.

15  
16 (34) Subramanian, S.; Ross, N. W.; MacKinnon, S. L., Myxinidin, a novel antimicrobial  
17 peptide from the epidermal mucus of hagfish, *Myxine glutinosa* L. *Mar. Biotechnol.*  
18 **2009**, *11*(6), 748-757.

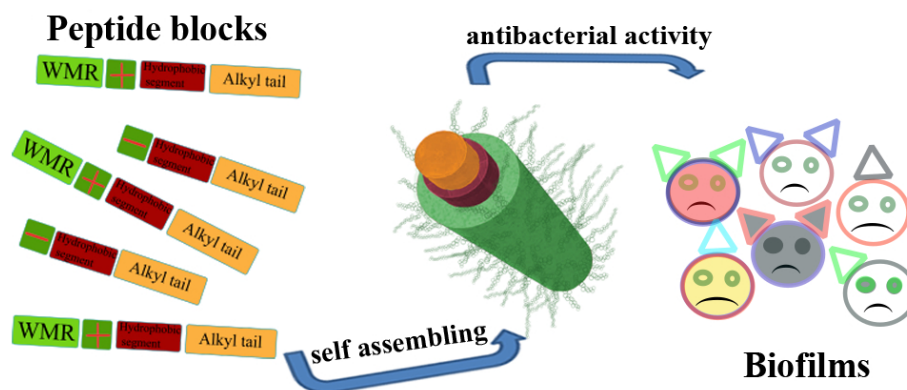
19  
20 (35) de Alteriis, E.; Maselli, V.; Falanga, A.; Galdiero, S.; Di Lella, F. M.; Gesuele, R.;  
21 Guida, M.; Galdiero, E., Efficiency of gold nanoparticles coated with the antimicrobial  
22 peptide indolicidin against biofilm formation and development of *Candida* spp. clinical  
23 isolates. *Infect. Drug Resist.* **2018**, *11*, 915-925.

24  
25 (36) de Alteriis, E.; Lombardi, L.; Falanga, A.; Napolano, M.; Galdiero, S.; Siciliano,  
26 A.; Carotenuto, R.; Guida, M.; Galdiero, E., Polymicrobial antibiofilm activity of the  
27 membranotropic peptide gH625 and its analogue. *Microb. Pathog.* **2018**, *125*, 189-195.

28  
29 (37) Rosenthal, V. D.; Al-Abdely, H. M.; El-Kholy, A. A.; AlKhawaja, S. A. A.;  
30 Leblebicioglu, H.; Mehta, Y.; Rai, V.; Hung, N. V.; Kanj, S. S.; Salama, M. F.; Salgado-  
31 Yopez, E.; Elahi, N.; Morfin Otero, R.; Apisarnthanarak, A.; De Carvalho, B. M.; Ider, B.  
32 E.; Fisher, D.; Buenaflor, M. C. S. G.; Petrov, M. M.; Quesada-Mora, A. M.; Zand, F.;  
33 Gurskis, V.; Anguseva, T.; Ikram, A.; Aguilar de Moros, D.; Duszynska, W.; Mejia, N.;  
34 Horhat, F. G.; Belskiy, V.; Mioljevic, V.; Di Silvestre, G.; Furova, K.; Ramos-Ortiz, G. Y.;  
35 Gamar Elanbya, M. O.; Satari, H. I.; Gupta, U.; Dendane, T.; Raka, L.; Guanche-  
36 Garcell, H.; Hu, B.; Padgett, D.; Jayatilleke, K.; Ben Jaballah, N.; Apostolopoulou, E.;  
37 Prudencio Leon, W. E.; Sepulveda-Chavez, A.; Telechea, H. M.; Trotter, A.; Alvarez-  
38 Moreno, C.; Kushner-Davalos, L., International Nosocomial Infection Control  
39 Consortium report, data summary of 50 countries for 2010-2015: Device-associated  
40 module. *Am. J. Infect. Control* **2016**, *44*(12), 1495-1504.  
41  
42  
43  
44  
45  
46  
47  
48  
49  
50  
51  
52  
53  
54  
55  
56  
57  
58  
59  
60

- 1  
2  
3  
4 (38) Percival, S. L.; Suleman, L., Slough and biofilm: removal of barriers to wound  
5 healing by desloughing. *J. Wound Care* **2015**, *24* (11), 498-510.  
6  
7 (39) Nobile, V.; Michelotti, A.; Cestone, E.; Caturla, N.; Castillo, J.; Benavente-García,  
8 O.; Pérez-Sánchez, A.; Micol, V., Skin photoprotective and antiageing effects of a  
9 combination of rosemary (*Rosmarinus officinalis*) and grapefruit (*Citrus paradisi*)  
10 polyphenols. *Food Nutr. Res.* **2016**, *60*, 31871-31886.  
11  
12 (40) Caporale, A.; Doti, N.; Sandomenico, A.; Ruvo, M., Evaluation of combined use  
13 of Oxyma and HATU in aggregating peptide sequences. *J. Pept. Sci.* **2017**, *23* (4), 272-  
14 281.  
15  
16 (41) Galdiero, S.; Capasso, D.; Vitiello, M.; Isanto, M.; Pedone, C.; Galdiero, M., Role  
17 of Surface-Exposed Loops of Haemophilus influenzae Protein P2 in the Mitogen-  
18 Activated Protein Kinase Cascade. *Infect. Immun.* **2003**, *71* (5), 2798-2809.  
19  
20 (42) Y. Shi; R. Lin; H. Cui; Azevedo, H. S., Multifunctional Self-Assembling Peptide-  
21 Based Nanostructures for Targeted Intracellular Delivery: Design, Physicochemical  
22 Characterization, and Biological Assessment. . *Chawla K. (eds) Biomaterials for Tissue*  
23 *Engineering. Methods in Molecular Biology. Humana Press, New York, NY* **2018**, *1758*.  
24  
25 (43) Aguiar, J.; Carpena, P.; Molina-Bolívar, J. A.; Carnero Ruiz, C., On the  
26 determination of the critical micelle concentration by the pyrene 1:3 ratio method. *J.*  
27 *Colloid Interface Sci.* **2003**, *258* (1), 116-122.  
28  
29 (44) Stepanovic, S.; Vukovic, D.; Hola, V.; Di Bonaventura, G.; Djukic, S.; Cirkovic, I.;  
30 Ruzicka, F., Quantification of biofilm in microtiter plates: overview of testing conditions  
31 and practical recommendations for assessment of biofilm production by staphylococci.  
32 *APMIS* **2007**, *115* (8), 891-899.  
33  
34 (45) Silva, S.; Pires, P.; Monteiro, D. R.; Negri, M.; Gorup, L. F.; Camargo, E. R.;  
35 Barbosa, D. B.; Oliveira, R.; Williams, D. W.; Henriques, M.; Azeredo, J., The effect of  
36 silver nanoparticles and nystatin on mixed biofilms of *Candida glabrata* and *Candida*  
37 *albicans* on acrylic. *Med. Mycol.* **2013**, *51* (2), 178-184.  
38  
39 (46) Fotakis, G.; Timbrell, J. A., In vitro cytotoxicity assays: Comparison of LDH,  
40 neutral red, MTT and protein assay in hepatoma cell lines following exposure to  
41 cadmium chloride. *Toxicol. Lett.* **2006**, *160* (2), 171-177.  
42  
43  
44  
45  
46  
47  
48  
49  
50  
51  
52  
53  
54  
55  
56  
57  
58  
59  
60

- 1  
2  
3  
4 (47) Castelletto, V.; Barnes, R. H.; Karatzas, K. A.; Edwards-Gayle, C. J. C.; Greco,  
5 F.; Hamley, I. W.; Rambo, R.; Seitsonen, J.; Ruokolainen, J., Arginine-Containing  
6 Surfactant-Like Peptides: Interaction with Lipid Membranes and Antimicrobial Activity.  
7 *Biomacromolecules* **2018**, *19* (7), 2782-2794.  
8  
9  
10 (48) Castelletto, V.; Barnes, R. H.; Karatzas, K. A.; Edwards-Gayle, C. J. C.; Greco,  
11 F.; Hamley, I. W.; Seitsonen, J.; Ruokolainen, J., Restructuring of Lipid Membranes by  
12 an Arginine-Capped Peptide Bolaamphiphile. *Langmuir* **2018**,  
13 DOI:10.1021/acs.langmuir.1028b01014.  
14  
15  
16 (49) Maiti, N. C.; Apetri, M. M.; Zagorski, M. G.; Carey, P. R.; Anderson, V. E., Raman  
17 Spectroscopic Characterization of Secondary Structure in Natively Unfolded Proteins:  
18  $\alpha$ -Synuclein. *J. Am. Chem. Soc.* **2004**, *126* (8), 2399-2408.  
19  
20  
21 (50) Hiemenz, P. E., Rajagopalan, R. , Principles of Colloid and Surface Chemistry,  
22 Revised and Expanded. *Boca Raton: CRC Press.* **1997**.  
23  
24  
25 (51) Meng, F.-G.; Zeng, X.; Hong, Y.-K.; Zhou, H.-M., Dissociation and unfolding of  
26 GCN4 leucine zipper in the presence of sodium dodecyl sulfate. *Biochimie* **2001**, *83*  
27 (10), 953-956.  
28  
29  
30 (52) Ghannoum, M. A.; Janini, G.; Khamis, L.; Radwan, S. S., Dimorphism-associated  
31 variations in the lipid composition of *Candida albicans*. *J. Gen. Microbiol.* **1986**, *132* (8),  
32 2367-2375.  
33  
34  
35 (53) Mason, A. J.; Marquette, A.; Bechinger, B., Zwitterionic Phospholipids and  
36 Sterols Modulate Antimicrobial Peptide-Induced Membrane Destabilization. *Biophys. J.*  
37 **2007**, *93* (12), 4289-4299.  
38  
39  
40 (54) Xu, D.; Jiang, L.; Singh, A.; Dustin, D.; Yang, M.; Liu, L.; Lund, R.; Sellati, T. J.;  
41 Dong, H., Designed supramolecular filamentous peptides: balance of nanostructure,  
42 cytotoxicity and antimicrobial activity. *Chem. Commun.* **2015**, *51* (7), 1289-1292.  
43  
44  
45  
46  
47  
48  
49  
50  
51  
52  
53  
54  
55  
56  
57  
58  
59  
60



graphical abstract

88x34mm (300 x 300 DPI)